Arabian Journal of Geosciences (2022) 15:1630
https://doi.org/10.1007/s12517-022-10875-z

ORIGINAL PAPER

The Upper Albian and Cenomanian–Turonian source rocks, and related oil seeps around Extrusive Triassic salt structures, Northern Tunisia: geochemical characterization and implication for petroleum system assessment

Ines Ghribi[1] · Anis Belhaj Mohamed[2] · Fares Khemiri[2] · Lassaad Ben Aissa[1] · Moncef Saidi[2] · Mohsen Layeb[3]

Received: 28 April 2022 / Accepted: 24 September 2022 / Published online: 21 October 2022

Abstract
The present paper deals with a geochemical investigation (TOC, Rock–Eval pyrolysis, and GC–MS) carried out on two potential mid-Cretaceous (Albian lower Fahdene and Cenomanian–Turonian Bahloul) source rocks and natural oil seeps collected from outcrops and mine boreholes located around the three extrusive salt structures of Ech-Cheid, Fej Lahdoum, and Boukhil, belonging to the Triassic domes zone of northern Tunisia. Rock–Eval pyrolysis results indicate the presence of moderate to good and moderate to excellent quantities of organic matter (OM) of oil–gas type II/III (means TOC: 0.90 wt.%, HI: 180 mg HC/g TOC, and PP: 2.00 mg HC/g rock) and oil-prone type II (means TOC: 3.5 wt.%, HI: 458 mg HC/g TOC, and PP: 20 mg HC/g rock) kerogens for the Fahdene and the Bahloul Formations (Fms), respectively. The thermal maturity of the OM preserved in these source rocks varies between late diagenesis and the late oil window depending mainly on the basin architecture marked by the presence of paleohighs (Triassic salt domes and horsts), grabens, half-grabens, and tilted blocks that controlled the varying degrees of subsidence. Gas chromatography-mass spectrometry (GC–MS) analysis of source rock extracts (Bitumen) and oil seeps and correlations with hierarchical cluster analysis (HCA) using biomarkers parameters (Diasteranes $C_{27}\beta\alpha S/C_{27}\alpha\alpha S$ and Hopanes $C_{29}H/C_{30}H$ ratios) suggest that the collected oil seep samples were sourced by the Fahdene and the Bahloul Fms. The spatio-temporal oil seeps distribution and associated tectonics indicate that several faults of NW–SE, N-S, E-W, and NE-SW trendings have facilitated oil migration from these source rocks to favorable reservoirs of middle-Turonian Bireno, Coniacian Douleb, and Campanian–Maastrichtian Abiod carbonates as well as a Miocene Oum Dhouil sandstone. These mid-Cretaceous source rocks and associated reservoirs, as well as overlaying argillaceous seals and traps (Flanks of diapirs, uplifted paleohighs, and anticlines), as essential elements, in addition to oil migration pathways and accumulation processes attest to the presence of active conventional petroleum systems in northern Tunisia. This could help guide petroleum exploration activities around subsurface diapir structures analogous.

Keywords Salt structures · Northern Tunisia · Mid-Cretaceous source rocks · Rock–Eval pyrolysis · Oil seeps · Biomarkers

Introduction

The Tethyan region is considered a major petroleum province where paleogeography and tectonic evolution have controlled the sedimentation and the development of essential elements for Mesozoic petroleum systems. In fact, the spatial distribution of source and reservoir rocks and their vertical stacking through time, as well as the trapping, maturation, expulsion, migration, accumulation, and preservation processes are closely related to the geodynamic evolution of the area. This was favored by widespread organic-rich sediments commonly called black shales that were deposited in

Responsible Editor: Santanu Banerjee

✉ Ines Ghribi
inesghribi1991@gmail.com

[1] Faculty of Sciences of Bizerte, University of Carthage, 7021 Jarzouna, Tunisia

[2] Entreprise Tunisienne d'Activités Pétrolières (ETAP), 54, Avenue Mohamed V-1002, Tunis, Tunisia

[3] University of Tunis, Higher Institute of Heritage Crafts, 5, al-Bashroush street, Montfleury, 1089 Tunis, Tunisia

most ocean basins during the Mesozoic worldwide oceanic anoxic events (Schlanger and Jenkyns 1976; Jenkyns 1988; Wignall and Myers 1988; Arthur et al. 1990; Cecca et al. 1994; Wignall 1994; Kuhnt et al. 1997; Barrett 1998; Sageman et al. 1998; Kuypers et al. 2002; Leckie et al. 2002; Luning and Kolonic 2003; Luning et al. 2004; Soua 2014a, b; Soua and Chihi, 2014; Talbi et al. 2018; Masrouhi et al. 2019; Talbi et al. 2021; Ben Ammar et al. 2021).

The most prominent of these oceanic anoxic events (OAEs) occurred in the Cretaceous such as the OAE1a (Selli event) (Elkhazri et al. 2013; Godet et al. 2014; Soua 2016; Talbi et al. 2018, 2021), OAE1b (Paquier event) (Bréhéret 1985; Khalifa et al. 2018), and OAE1d (Breistroffer event) (Schlanger and Jenkyns 1976; Talbi 1991), respectively, during early and late Albian, and OAE2 (Bonarelli event) at the Cenomanian–Turonian boundary (e.g. Arthur et al. 1988; Soua et al. 2022). Smaller-scale events of probably regional extent were also identified in several basins such as the middle Albian OAE1c and Coniacian-Santonian OAE3 (Burnett 1996; Arenillas et al. 2000; Jenkyns 2010; Ben Fadhel et al. 2011; Talbi et al. 2021; Ben Ammar et al. 2021).

These Cretaceous oceanic anoxic events (OAEs) are at the origin of the development, especially, of the Albian and Cenomanian–Turonian (C/T) world-class source rocks recorded in the northern African domain (Fig. 1b and c) (Arthur et al. 1990; Luning and Kolonic 2003; Luning et al.

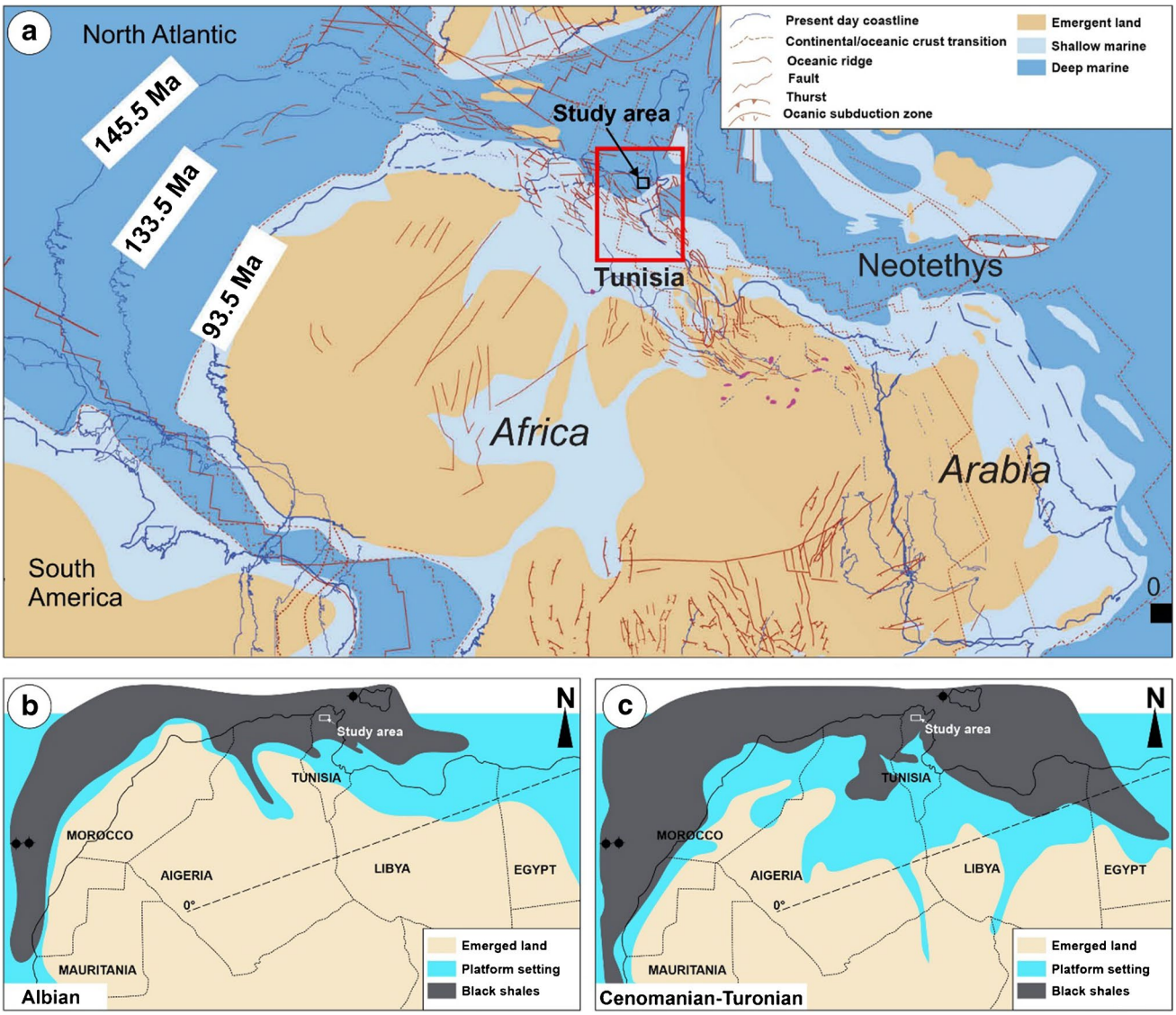

Fig. 1 **a** Paleogeographic reconstruction map of the western Tethyan domain during the early Cretaceous and Cenomanian–Turonian transition. Reconstructions were made after Barrier and Vrielynck 2008 and Tribovillard et al. 2012 **b** Albian and **c** late Cenomanian–early Turonian in North Africa. Data were compiled from Luning et al. 2004; Zghal and Arnaud-Vanneau 2005; Baudin 2005; Reichelt 2005; Bodin et al. 2006; Chihaoui 2008; Jenkyns 2010; Ben Fadhel et al. 2011; Tribovillard et al. 2012

2004; Soua 2014a, b; Soua and Chihi, 2014; Soua 2015; Talbi et al. 2018). These C/T with the other mid-Cretaceous source rocks have sourced almost one-third of the world's HC reserves (Klemme and Uimishek, 1991; Luning et al. 2004).

In the southern Tethyan margin, namely in Tunisia and Algeria, the deposition of Cretaceous organic-rich sediments is strongly controlled by the development of (1) half-graben systems that occurred during the opening of the central and southern Atlantic oceans and the counter-clockwise rotation of African plate (Dercourt 2005; Scotese 2007; Fig. 1a), and (2) Triassic diapiric extrusion movements related to the global paleogeographical evolution during the Cretaceous, which succeeded the break-up of the Pangea supercontinent (Ziegler 1988; Veevers et al. 1994; Veevers 2004; Withjack et al. 1998; Golonka and Ford 2000; Golonka et al. 2002; Soua 2014a).

In Tunisia, the main Cretaceous-OAEs are recorded within the Albian lower Fahdene and the late Cenomanian-early Turonian Bahloul Fms (e.g. Talbi 1991; Saidi 1993; Luning et al. 2004; Affouri et al. 2013; Layeb et al. 2013; Soua 2015; Talbi et al. 2018; Ben Ammar et al. 2021; Talbi et al. 2021). These source rocks are proven as the main sources of hydrocarbons for many petroleum discoveries such as the onshore and offshore fields in central Tunisian Altas as well as the foreland basins of the Pelagian domain (e.g. Yukler et al. 1994; Saidi et al. 1998; Bédir et al. 2001; El Euchi et al. 2004; Klett 2022). However, previous basin modeling and geochemical studies (El Euchi et al. 2004; Mejri et al. 2006; Bédir et al 2020) showed that the most prolific organic-rich series are essentially represented by the Cenomanian–Turonian time interval.

These mid-Cretaceous source rocks are associated with several carbonate reservoirs (the Aptian Serdj, the Turonian-Coniacian Bireno and Douleb Fms, and the Campanian–Maastrichtian Abiod Fm; Ben Chaabane et al. 2018; Bédir et al. 2020; Soltani et al. 2022) and argillaceous seals (the Albian Fahdene, the upper Turonian-Santonian Aleg, and the Paleocene El Haria Fms). The most favorable traps, as recognized in the Sahel and Pelagian block basins, are mainly constituted by anticline structures, horsts, apex of titled blocks and locally Triassic salt domes/diapirs (e.g. Rabhi and Ben Ayed 1990; Masrouhi et al. 2008; Khomsi et al. 2009).

Therefore, successive tectonic events and halokinetic movements are generally responsible for the presence of numerous hydrocarbon seepages in northern Tunisia, especially in the diapir province (Belayouni et al. 1992; Belhaj Mohamed et al. 2015; Hallek and Montacer 2021).

In this context, special attention was given to the seepages identified during the fieldwork. Additionally, the aforementioned source rocks, reservoirs, seals, and Triassic salt dome traps, qualify this area as an important potential petroleum location for oil exploration. However, despite the notable efforts deployed in the evaluation of the petroleum potential of the upper Albian and the Cenomanian–Turonian source rocks in different regions of northern and eastern Tunisia, only a little attention was focused on their role as essential elements of active petroleum systems around Triassic salt domes structures.

The present work presents the first detailed geochemical investigation carried out on potential Cretaceous (Albian and Cenomanian–Turonian) source rocks and oil seeps belonging to the Triassic domes zone of northern Tunisia. It aims to (1) evaluate the ability of these source rocks to generate hydrocarbons and their possible genetic relation with the collected oil seeps, and (2) better understand the functioning of the region's petroleum systems with special attention to the interplay between source rocks, reservoirs, and tectonics as possible hydrocarbon migration pathways.

Regional geology

Tunisia is located in the northeast part of the Maghreb domain which exposes numerous parallel structural trends bordered by major tectonic boundaries (Fig. 2a) where each zone is characterized by a proper deformation style. Four structural zones have been recognized in Tunisia (Fig. 2b and c): (1) the thrust belt with allochthonous to para-autochthonous highly folded and faulted upper Cretaceous to Eocene and Oligo-Miocene thrust sheet sediments (Rouvier 1977; Khomsi et al. 2009; Riahi et al. 2021), (2) the Tellian Medjerda molassic basin with fore-deep flexural subsidence and thick post-Atlassic sedimentation (Melki et al. 2012; Bejaoui et al. 2017), (3) the salt diapirs zone with NE–SW trending structures defining the "saliferous province" (e.g. Talbot 2005; Hamdi Naser et al. 2009), and (4) the Atlas zone marked by NE-SW trending asymmetric faulted folds (Masrouhi et al. 2013; Amri et al. 2020).

The northern Tunisian basin, belonging to the Atlas zone, was segmented into NE–SW trending tilted blocks that controlled the organic-rich strata deposition (Melki et al. 2012). At least four major NE–SW master faults have controlled differential subsidence and sedimentation patterns since the early Cretaceous. These faults formed weak zones for salt movement and doming and have been reactivated later for several times until the late Eocene and during the Miocene Alpine and Atlassic phases causing more complex salt diapir structures (Perthuisot 1978; Zargouni 1978; Bouaziz et al. 2002; Masrouhi et al. 2008; Khomsi et al. 2009; Melki et al. 2012).

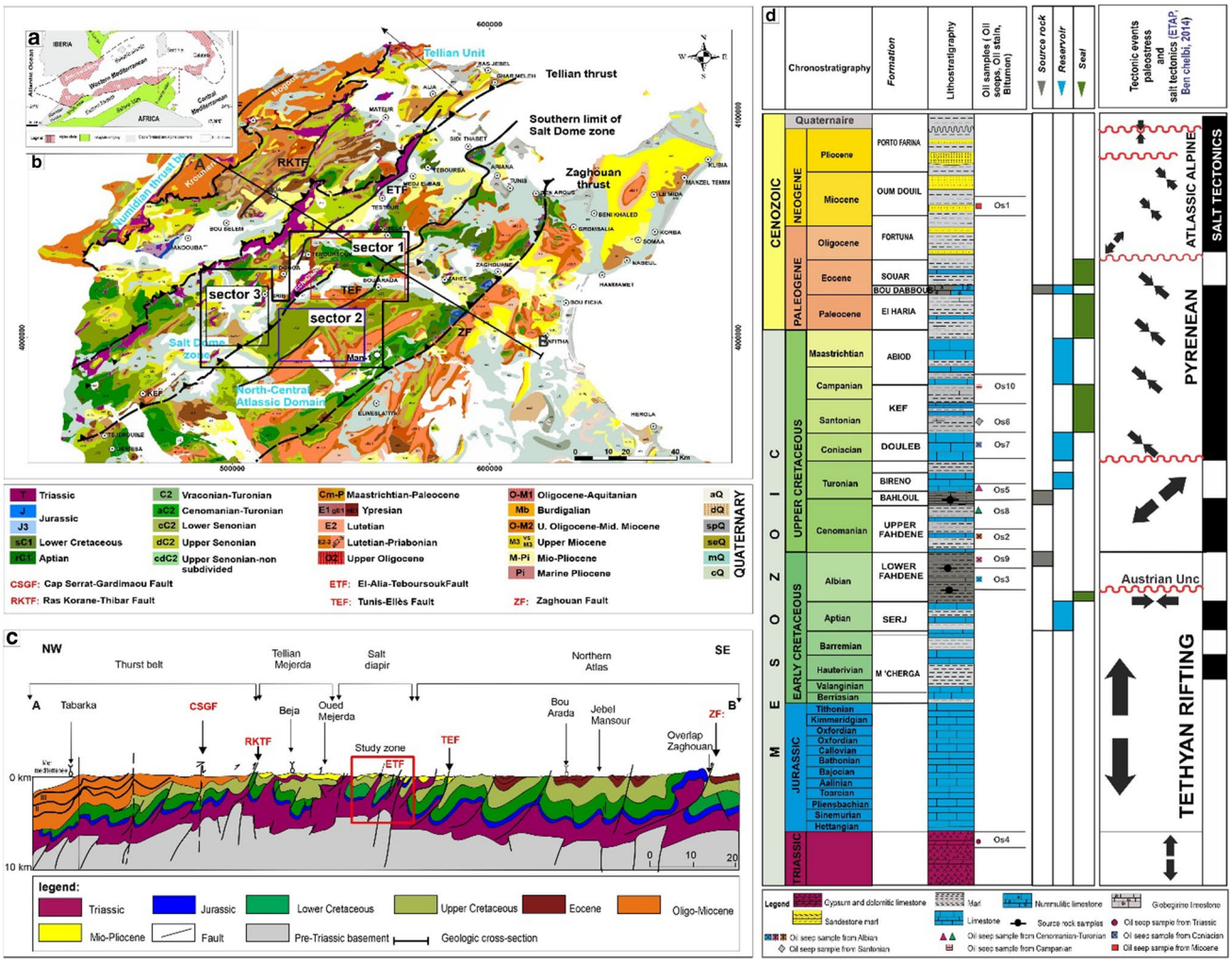

Fig. 2 **a** The studied area within its regional geodynamic Mediterranean context (redrawn after Durand-Delga 1980). **b** Detailed geologic maps compiled from 1/50,000 geological maps (Dali 1994; Mahjoub and Dali 1998) showing the location of the studied area; **c** NW–SE synthetic and interpretative cross-section in northern Tunisia from the Alpine domain crossing the Atlas domain to the eastern Atlas foreland. Cross-section modified from Khomsi et al. 2009 and Martinez and Truillet 1987. **d** Synthetic stratigraphic chart of northern Tunisia based on the Tunisian Stratigraphic Chart (Ben Chalbi 2014, ETAP 2010) showing the position of the studied oil seep samples

Local geology

Structural context

The studied area, located in the south of Teboursouk village (Fig. 2b), covers the central part of the saliferous province occupied by the three Triassic salt domes of Ech-Cheid (Fig. 2b; sectors 1 and 2), Fej Lahdoum, and Boukhil (Fig. 2b; sector 3). These salt domes pertain to the Atlas foreland which is an intensely fractured zone owing to the succession of many tectonic events (Rouvier 1977; Durand-Delga 1980; Ben Ayed 1993; Melki et al. 2011). This is affected by strike-slip and thrust faults trending E-W, N-S, and NE–SW (Ben Ayed 1994; Vila 1995; Masrouhi et al. 2013).

Some authors (Jauzein 1967; Perthuisot 1978) emphasize a NE–SW major alignment formed by regional faults organized in a relay (the major Teboursouk overthrust) (Perthuisot 1978; Zargouni 1978). Later, Adil (1993) stated that this fault trend is the tectonic heritage from the Tethys opening. The tectonic faults are reactivated in strike-slip with conjugated structures in push-up and pull-apart. This fault system has facilitated the uplift of the Triassic material and the establishment of the Triassic piercing into the Mesozoic and Cenozoic coverage. However, in some previous works, the halokinetic movement in the region has occurred

in two major periods: first doming during the Aptian times (Perthuisot 1978) and a second during middle Eocene times which is the probable period of surface piercing (Perthuisot 1978). The last Atlassic compression sculpted the definitive and actual Triassic structures and diapirs.

The El Alia-Teboursouk NE-SW trending master fault, recognized in the studied domain, represents one of these previously cited master faults which have a significant impact on sedimentation expressed by normal faulting that continued during the Cretaceous-Miocene interval, creating paleohighs and subsiding blocks (Bouaziz et al. 2002, Khomsi et al. 2006, Masrouhi et al. 2008, Frizon de Lamotte and Mouchard 2009, Melki et al. 2010, Melki et al. 2011; Fig. 2). This architecture is strongly witnessed by the obvious thickness and facies variations.

Post-relaxation normal faulting was observed in salt-cored anticlines in the whole area and gives more complexity to structures. These structures constitute a weak zone that allowed an easy migration of oil to the surface along faults and fractures. The main pathways for oil migration are considered to be controlled by the regional tectonic movements along NW–SE, N-S, E-W, and NE-SW trending normal faults (present work).

Lithostratigraphy

The lithostratigraphic column of outcropping strata is composed of two main sedimentary series (Mejri et al. 2006; ETAP 2010; Ben Chalbi et al. 2014; Arfaoui et al. 2018; Fig. 2d).

(1) The Mesozoic strata comprise the following lithostratigraphic units:

The Triassic series of Ech-Cheid, Fej Lahdoum, and Boukhil domes consist of thick clay, dolomite, and evaporites intercalated by thin clay beds. The Jurassic series are dominated by nodular and siliceous limestones and marls. The early Cretaceous shales, marls, and thin clastic turbidites strata of M'Cherga Fm are followed by the late Aptian–early Albian sediments constituted by black clayey marls, sands, and fossiliferous limestone alternations. The mid-upper Albian Fahdene Fm which is one of the main potential source rocks was firstly described in the type locality of Oued Bahloul located to the south of Kesra village in central Tunisia (Burollet 1956) and consists of cyclic thinly laminated limestones alternating with marls and shales (Burollet 1956; Talbi 1991; Saidi 1993; Soua 2015). This formation constitutes the lateral equivalent of the shallow-marine carbonate/evaporite succession of the Zebbag Fm, developed in central-southern Tunisia (Soltani et al. 2022). The late Cretaceous is dominated by pelagic carbonates and marls of Cenomanian upper Fahdene member. It is followed by the late Cenomanian-early Turonian black shales and laminated limestones. The organic-rich Cenomanian–Turonian deposits in north-western, North-central, and Eastern Tunisia are generally composed of about 30–40 m thick of well-bedded dark grey to black bituminous limestone, with common local intercalations of marls and argillaceous limestone, and specify the Bahloul Fm (Burollet 1956; Layeb 1990; Saidi 1993; Soua 2015; Bachari et al. 2019; Hadded et al. 2021). The mode of arrangement of these facies highlighted the presence of three lithological units (U_1, U_2, and U_3) of a regional correlating value (Layeb and Belyouni, 1989; Layeb et al. 2013; Touati and Haji 2018). The lower unit (U_1) is majorly formed by laminated limestone commonly called black shale alternating with one to three marl levels and one or two beds of radiolarian siliceous limestone. The middle unit (U_2) is characterized by the presence of four marl beds alternating with laminated black shale. The upper unit (U_3) is composed of mainly less laminated limestone alternating with well-laminated black shale levels. This latter is overlaid by Turonian limestone beds of the Bireno member. Coniacian-Santonian marls and limy beds overlie the previous sequence. The upper Campanian-lower Maastrichtian deposits are represented by the Abiod Fm with alternations of white chalky limestones and marls.

(2) The Cenozoic interval is composed of Paleocene marls rich in pelagic micro-fauna corresponding to El Haria Fm, Eocene limestones rich in nummulites (El Garia Fm.), and their equivalent globigerina organic-rich limestones (Bou Dabbous Fm). These deposits are related to the partial emersion of Jebel Ech-Cheid at the end of the Cretaceous period and which continued until the end of Eocene (Perthuisot 1978). Oligocene deltaic deposits are formed of siliceous sandstones (sandstone nodules), unconformably overlain by Miocene marls and post-Atlassic orogeny Pliocene–Quaternary continental conglomeratic beds.

Regarding the structural styles and deformations, we notice the importance of salt anomalies forming initial doming with at least two angular unconformities. These unconformities fossilize the main folding related to events previously described above. In addition, younger sediments unconformably overlay salt at the core and look like perched synclines. Such features outline a clear continuous salt activity and extrusion from both sides allowing a kind of flexural synform as is the case of the Jebel Ech-Cheid anticline.

At more advanced deformation salt anomalies evolve into diapirs injected along reverse faulting and thrusting. In fact, structures become more complex with detachment Triassic levels, folding and verticalized to reversed dipping strata like in Fej Lahdoum and Boukhil.

Material and methods

Samples

A total of 131 source rock and 10 oil seep samples, collected from three different sectors (sectors 1, 2, and 3) and different stratigraphic levels around the Ech-Cheid salt dome, were analyzed using Rock–Eval pyrolysis (RE-6) and biomarkers (GC–MS).

Source rock samples were collected from the lower Fahdene (52 samples) and the Bahloul (79 samples) Fms of different outcrop sections (Fig. 3; Table 1) located in sectors 1 and 2, while hydrocarbon seepages corresponding to oil stains, seeps mixed with water, asphalts and bitumen in the fresh break were taken from fractures/faults within the three sectors (Table 2; Figs. 4 and 5).

The first sector (sector 1) represents the northeastern Ech-Cheid outcrops (Fig. 3a) with main lower Fahdene sections at Oued Siliana (OS-LF) and Jebel Rihane (JR-LF), and Bahloul sections from Oued Siliana (OS-BH) and Kenana (KN-BH) outcrops. Three oil seep samples located North-Est of Ech-Cheid were collected (Rous-Essouani: OS1, Oued Siliana: OS2, Jebel Rihane: OS3). They consist of black material mixed with water or sample and from fractures in fresh breakage (Table 2, Fig. 5a, section AA' of Ben Slama 2011).

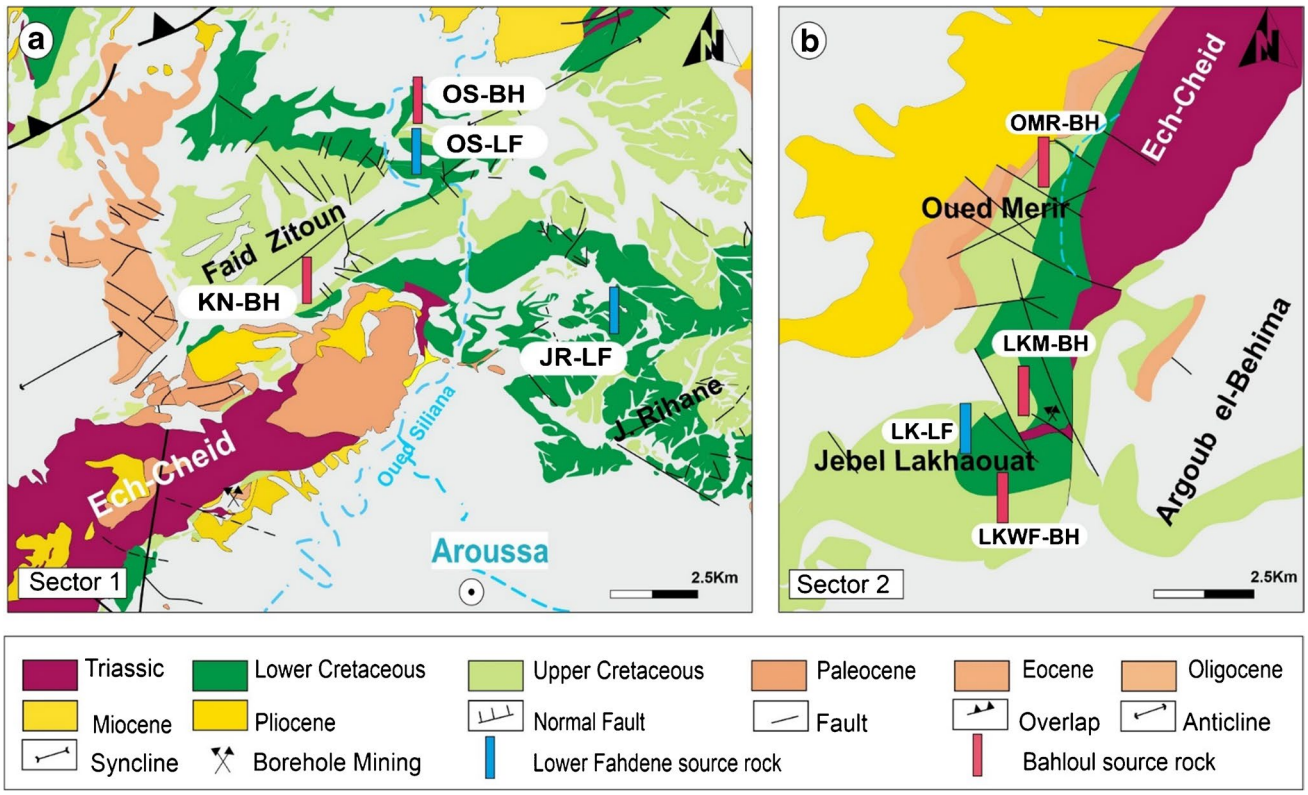

Fig. 3 **a** Detailed geologic map of sector 1 from geological 1/50,000 map of Teboursouk (Perthuisot 1974) and **b** Detailed geologic map of sector 2 from geological 1/50,000 map of Gaafour (Dali 1994; Mahjoub and Dali 1998) showing the location of source rock samples

Table 1 Designation and geographic coordinates of the studied source rocks

Source rock sampling	Designation	Short name	Formation	Coordinates (m)	
North Ech-Cheid (Sector 1)	Jebel Rihane	JR-LF	Lower Fahdene	X=547135.348	Y=4035631.682
	Oued Siliana	OS-LF/OS-BH	Lower Fahdene (LF)/Bahloul (BH)	X=545141.804	Y=4036279.23
	Kenana	KN-BH	Bahloul	X=531337.543	Y=4029641.597
South Ech-Cheid (Sector 2)	Lakhaouat	LK-LF/LKWF-BH/LKM-BH	Lower Fahdene	X=519855.562	Y=4014244.354
	Oued Merir	OMR-BH	Lower Fahdene (LF)/Bahloul (BH)	X=521382.287	Y=4017887.028

Table 2 Location, short names, and geographic coordinates of the studied oil seep samples

Geological Sector	Oil seep sample locality	Short name	Host formation/ Age	Location	Description of samples	Coordinates (m)	
North Ech-Cheid (Sector 1)	Rous Essouani	OS1	Triassic/Miocene	Jebel Ech-Cheid	Oil seep is sampled from water source in the Triassic-Miocene contact	$X=536,519.165$	$Y=4,028,279.469$
	Oued Siliana	OS2	Albian	Fault	Oil stain within limestone fractures	$X=541,132.615$	$Y=4,034,564.201$
	Jebel Rihane	OS3	Albian	Fault	Oil stain within limestone fractures	$X=546,753.318$	$Y=4,035,903.543$
South Ech-Cheid (Sector 2)	Trias outcrop	OS4	Triassic/LateTertiary contact	In situ	A sample is extracted from the Triassic sediments of Ech-Cheid	$X=521,821.962$	$Y=4,016,113.309$
	Lakhaouat	OS5	Turonian	Mining borehole	Bitumen within a mining core of Lakhaouat mine (South of Ech-Cheid)	$X=520,256.322$	$Y=4,014,962.468$
	Oued Behima	OS6	Santonian	Fracture	Oil stain within limestone fractures	$X=531,839.075$	$Y=4,015,882.588$
	Sidi Bilel	OS7	Coniacian	Fracture	Oil stain within limestone fractures	$X=528,192.579$	$Y=4,011,081.574$
	Argoub Ettela	OS8	Turonian	Fracture	Oil stain within fractures in limestone beds	$X=532,965.992$	$Y=4,012,417.656$
West Ech-Cheid (Sector 3)	Fej Lahdoum	OS9	Triassic/Cretaceous	Mining borehole	Bitumen within a mining core from Fej Lahdoum mine (West of Ech-Cheid)	$X=508,964.96$	$Y=4,025,945.844$
	Boukhil	OS10	Campanian	Mining borehole	Bitumen within a mining core from Boukhil mine (West of Ech-Cheid)	$X=510,531.212$	$Y=4,015,569.278$

In sector 2, located in the South-West of Ech-Cheïd and Lakhaouat outcrops (Fig. 3b), samples were collected from the Lakhaouat section (LK-LF) for lower Fahdene Fm and from Lakhaouat West Flank (LKWF-BH), Lakhaouat mine (LKM-BH), and Oued Merir section (OMR-BH) for Bahloul Fm (Table 1). Five oil seeps were sampled here at the surface from Triassic evaporites (OS4) and Santonian (OS6), Coniacian (OS7), and Turonian (OS8) carbonates (Fig. 5b). Most prominently, bitumen is found filling fresh breakage or fractures. One sample is collected from the borehole mining core in Lakhaouat Mine (OS5) from Turonian carbonate facies (Table 2, Fig. 5b, section BB' of Ben Slama 2011).

In sector 3, two samples were collected from Fej Lahdoum (OS9) and Boukhil (OS10) mines, respectively from the Albian to Cenomanian Fahdene borehole core carbonates and the Campanian to Maastrichtian Abiod Fm (Fig. 5c, Table 2).

TOC analysis and Rock–Eval pyrolysis

Total organic carbon (TOC) and Rock–Eval pyrolysis were performed on 70 mg of the crushed rock sample using a Rock–Eval 6 instrument equipped with a TOC module (IFP Rock–Eval methods). The samples were first heated from

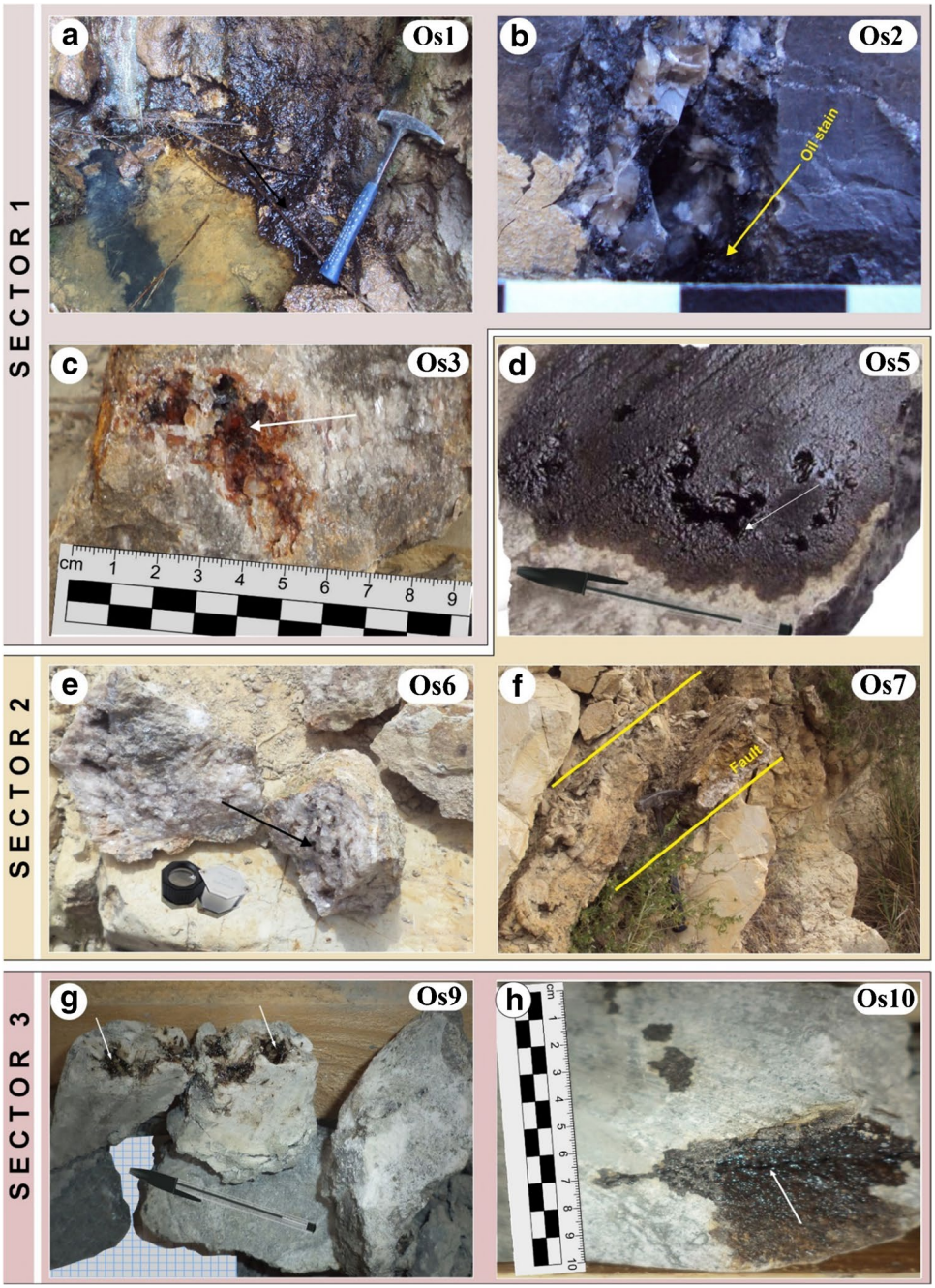

Fig. 4 Photos illustrating the selected oil seep samples from the study area, in sector 1: **a** oil seep hosted in the Triassic-Miocene contact mixed with water in Rous Souani; **b** sample from the Albian carbonate facies of Fahdene formation along the fault in Oued Siliana; **c** sample from the Albian carbonate facies along the fault in Jebel Rihane; and from sector 2: **d** sample from the Turonian carbonate facies in Lakhaouat mine; **e** sample from the Santonian carbonate facies along the fault in Oued Behima; **f** sample from the Coniacian carbonate facies along the fault in Sidi Bilel; from sector 3: **g** sample from the Albian carbonate facies in Fej Lahdoum; **h** sample from the Campanian carbonate facies in Boukhil mine (see arrows and references therein)

300 to 650 ºC (at 25 °C/mn) in a nitrogen atmosphere in order to quantify the free hydrocarbons (S_1: mg HC/g rock), the potential hydrocarbons (S_2: mg HC/g rock), carbon dioxide expelled during pyrolysis of kerogen (S_3: mg CO_2/g rock), and the temperature of maximum yield of pyrolysis (T_{max} °C). The residual carbon is obtained during the oxidation cycle of the already pyrolyzed sample (heated from 300 to 800 °C) by summing the organic carbon oxidized into CO (S_4 CO peak) and CO_2 (S_4 CO_2 peak). The total organic carbon (TOC) is then determined by the summation of pyrolyzed carbon (PC: 0.083 ($S_1 + S_2$)) and residual carbon (RC: S_4/10). Several additional parameters including HI (hydrogen index: $S_2 \times 100$/TOC), OI (oxygen index: $S_3 \times 100$/TOC), and PI (production index: $S_1/(S_1 + S_2)$) (Behar et al. 2001) were calculated.

Bitumen extraction

Source rock extracts were obtained from six selected samples: three samples from the lower Fahdene source rock (JR-LF-9 and OS-LF-4 from sector 1, and LK-LF-5 from sector

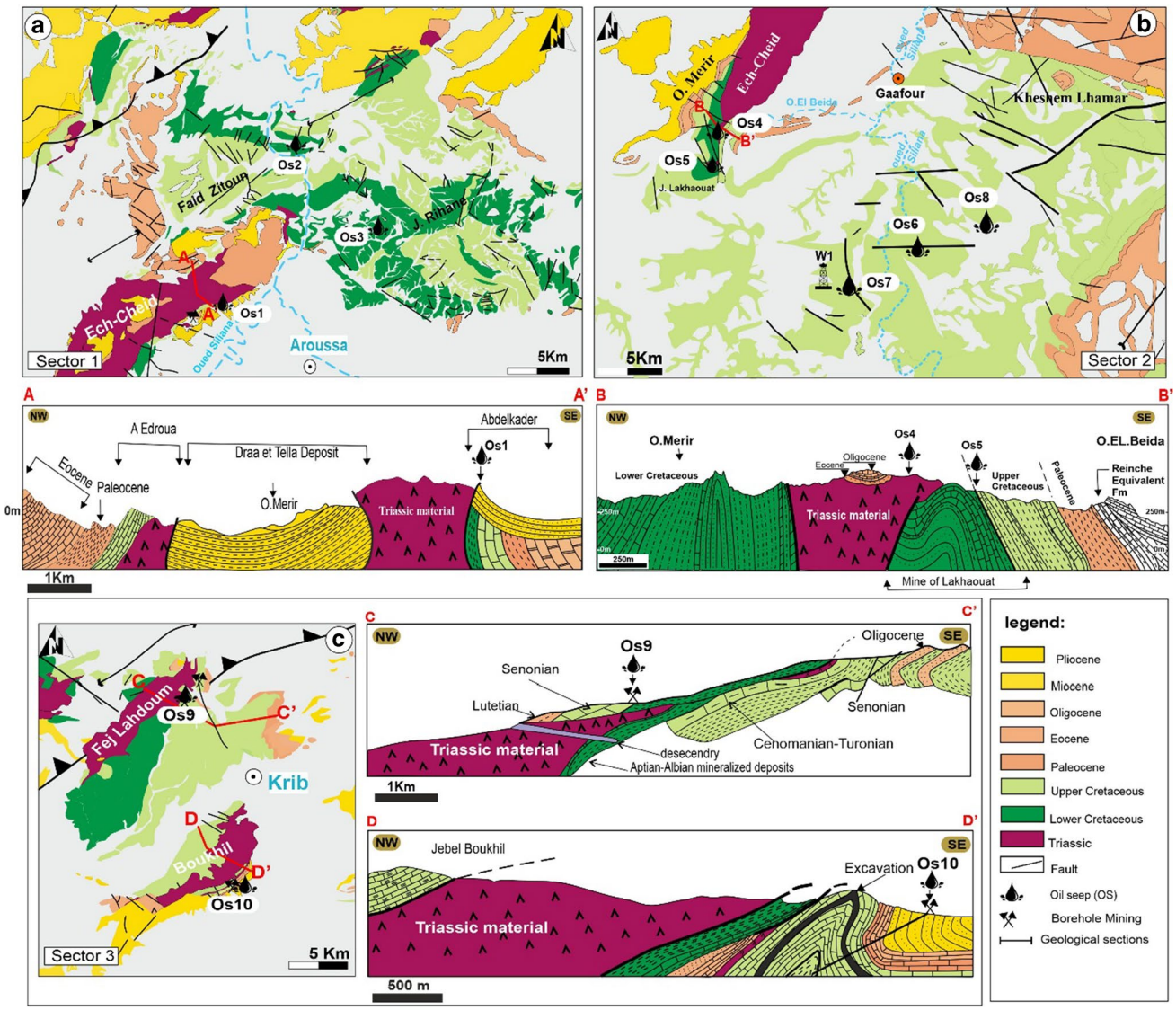

Fig. 5 **a** Detailed geologic map from geological 1/50000 map of Teboursouk (Perthuisot 1974) with (AA') geological cross-section in North Ech-Cheid (Ben Slama 2011) showing the location of oil seep samples from sector 1. **b** Detailed geologic map from geological 1/50,000 map of Gaafour (Dali 1994; Mahjoub and Dali 1998) with (BB') geological cross-section in North Ech-Cheid (Ben Slama 2011) showing the location of oil seep samples from sector 2. **c** Detailed geologic map compiled from geological 1/50,000 map of Teboursouk (Perthuisot 1974) and Gaafour (Dali 1994; Mahjoub and Dali 1998) with (CC') geological cross-section of Fej Lahdoum and Boukhil outcrops showing the location of oil seep samples from sector 3

2) and three others from the Bahloul source rock (OS-BH-33 from sector 1 and LK-BH-2, and OMR-BH-3 from sector 2).

The $C_{15}+$ soluble organic matter (SOM) or source rock extract (EOM) was solvent-extracted with dichloromethane (CH_2Cl_2) in a Soxhlet apparatus using cellulose thimbles (12 h). Rapid extraction was performed for the oil seep to separate the organic fraction from the rest of the rock with a mixture of dichloromethane and methanol (90: 10 vol %) for 72 h using a Soxhlet extraction apparatus. The solution containing the EOM was rotary evaporated to a smaller volume and preserved in a 4 ml vial for asphaltene precipitation and fractionation into aliphatic and aromatic hydrocarbons and polar compounds.

Total extracts were separated into saturate, aromatic, and NSO-compounds fractions by liquid chromatography using a mini-column (Pasteur Pipette) packed with activated silica gel. These were eluted using nC_5/CH_2Cl_2 (65/65, V/V) and CH_2Cl_2/methanol (90/10, V/V), respectively.

Biomolecular GC–MS

GC–MS analyses were conducted on the saturated and aromatic fractions in the oil seeps and source rock extracts (Bitumen) using an Agilent 7683B quadrupole mass-spectrometer coupled to a 7890A gas chromatograph. The gas chromatograph was equipped with a DB-1MS fused silica capillary column of 60 m in length, 0.25 mm i.d., and 0.25 µm film thickness. Helium was used as the carrier gas with a flow rate of 1 ml/mn. The oven temperature was programmed from 50 (hold time 10 mn) to 170 °C (hold time 15 mn) at 5 °C/min, to 300 °C (hold time 24 mn) at 1.5 °C/mn. The mass spectrometer was operated in EI mode at ionization energy of 70 eV and a source temperature of 300 °C. The biomarker contents were determined (Table 5) using single ion monitoring *n*-alkanes (*m/z* 85), terpanes (*m/z* 191) (Table 3), steranes (*m/z* 217), and triaromatic steroids (*m/z* 231).

Hierarchical cluster analysis

Hierarchical cluster analysis (HCA) was performed in order to group the oil seep samples and oil with source rock s. The analysis was completed using autoscale preprocessing and Euclidean metric distance following the method of Ward (1963). The analysis included different selected biomarkers.

Results

Rock–Eval pyrolysis of potential source rocks

Lower Fahdene Fm

The geochemical log presented in Fig. 6 summarizes the total organic carbon (TOC) content and Rock–Eval parameters related to the lower Fahdene samples collected from sector 1. About 50% of the samples have TOC content higher

Table 3 Peak assignment for Triterpanes (*m/z* 191), Steranes (*m/z* 217), and aromatic biomarkers (*m/z* 231) of oil seeps samples from GC–MS chromatograms based on Philip (1985) and Peters and Moldowan (1993)

Peak ID	Terpanes GC/MS *m/z* 191	Peak ID	Steranes GC/MS *m/z* 217
1	Tricyclic Terpane C_{19} (C_{19}T)	A	C_{27}βαS: 13β, 17α, 20S-Diacholestane
2	Tricyclic Terpane C_{20} (C_{20}T)	B	C_{27}βαR: 13β, 17α, 20R-Diacholestane
3	Tricyclic Terpane C_{21} (C_{21}T)	E	C_{28}βαS: 13β, 17α, 20S-Methyldiacholestane
4	Tricyclic Terpane C_{22} (C_{22}T)	F	C_{28}βαR:13β,17α, 20R-Methyldiacholestane
5	Tricyclic Terpane C_{23} (C_{23}T)	G	C_{27}ααS: 5α,14α(H),17α(H)-20S-Cholestane
6	Tricyclic Terpane C_{24} (C_{24}T)	H	C_{27}ββR: 5α,14β,17β,20R-Cholestane
7	Tricyclic Terpane C_{25} (C_{25}T)	J	C_{27}ββS: 5α,14α,17α,20S-Cholestane
8	Tetracyclic Terpane C_{24} (C_{24}TeT)	K	C_{27}ααR: 5α,14α,17α,20R-Methylcholestane
9	Tricyclic Terpane C_{26} (C_{26}T)	L	C_{29}βαR: 13β,17α,20R-Ethyldiacholestane
10	Tricyclic Terpane C_{28} (C_{28}T)	M	C_{28}ααS: 5α,14α,17α,20S-Ethylcholestane
11	Tricyclic Terpane C_{29} (C_{29}T)	N	C_{29}αβR: 5α,14α(H),17β(H)-20R-24-Ethylcholestane
12	18α(H)-22,29,30-trisnorneohopane (Ts)	O	C_{28}ββR: 5α,14α,17α,20R-Ethylcholestane
13	17α(H)-22,29,30-trisnorhopane (Tm)	P	C_{28}ββS: 5α,14β(H),17β(H)-20S -24-Methylcholestane
14	TricyclicTerpane C_{30} (C_{30}T)	Q	C_{28}ααR: 5α,14α(H),17α(H)-20R -24-Methylcholestane
15	17α(H),21β(H)-norohopanes (C_{29} H)	R	C_{29}ααS: 5α(H),14α(H),17α(H)-20S-24-Ethylcholestane
16	18α(H)-norneohopane (C_{29}Ts)	S	C_{29}ββR: 5α(H),14β(H),17β(H)-20R-24-Ethylcholestane
17	C30 17α(H)-diahopane (d30)	T	C_{29}ββS: 5α(H),14α(H),17α(H)-20S-24-Ethylcholestane
18	117β(H),21α(H)-normoretane (C_{29}M)	U	C_{29}ααR: 5α(H),14β(H),17β(H)-20S-24-Ethylcholestane
19	19: 17α(H),21β(H)-hopane (C_{30}H)	**Peak ID**	**Triaromatic steroid GC/MS *m/z* 231**
20	20: 17β(H),21α(H)-moretane (C_{30}M)	TA20	$C_{20}H_{20}$Triaromaticsteroid
21	21: 17α(H),21β(H)-C_{31}homohopane (22S + 22R)	TA21	$C_{21}H_{22}$Triaromaticsteroid
22	22:Gammacerane; pentacyclicterpane (C30H52)	TA26S	$C_{26}H_{32}$Triaromaticcholestane 20S
23	23: 17α(H),21β(H)-C_{32}bishomohopane (22S + 22R)	TA26R + 27S	$C_{26}H_{32}$ + $C_{27}H_{34}$Triaromatic cholestane 20R + triaromatic ergostane 20S
24	24: 17α(H),21β(H)-C_{33}trishomohopane (22S + 22R)	TA28S	$C_{28}H_{36}$Triaromaticstigmastane 20S
25	25: 17α(H),21β(H)-C_{34}tetrakishomohopane (22S + 22R)	TA27R	$C_{27}H_{34}$Triaromaticergostane 20R
26	26: 17α(H),21β(H)-C_{35}pentakishomohopane (22S + 22R)	TA28R	$C_{28}H_{36}$Triaromaticstigmastane 20R

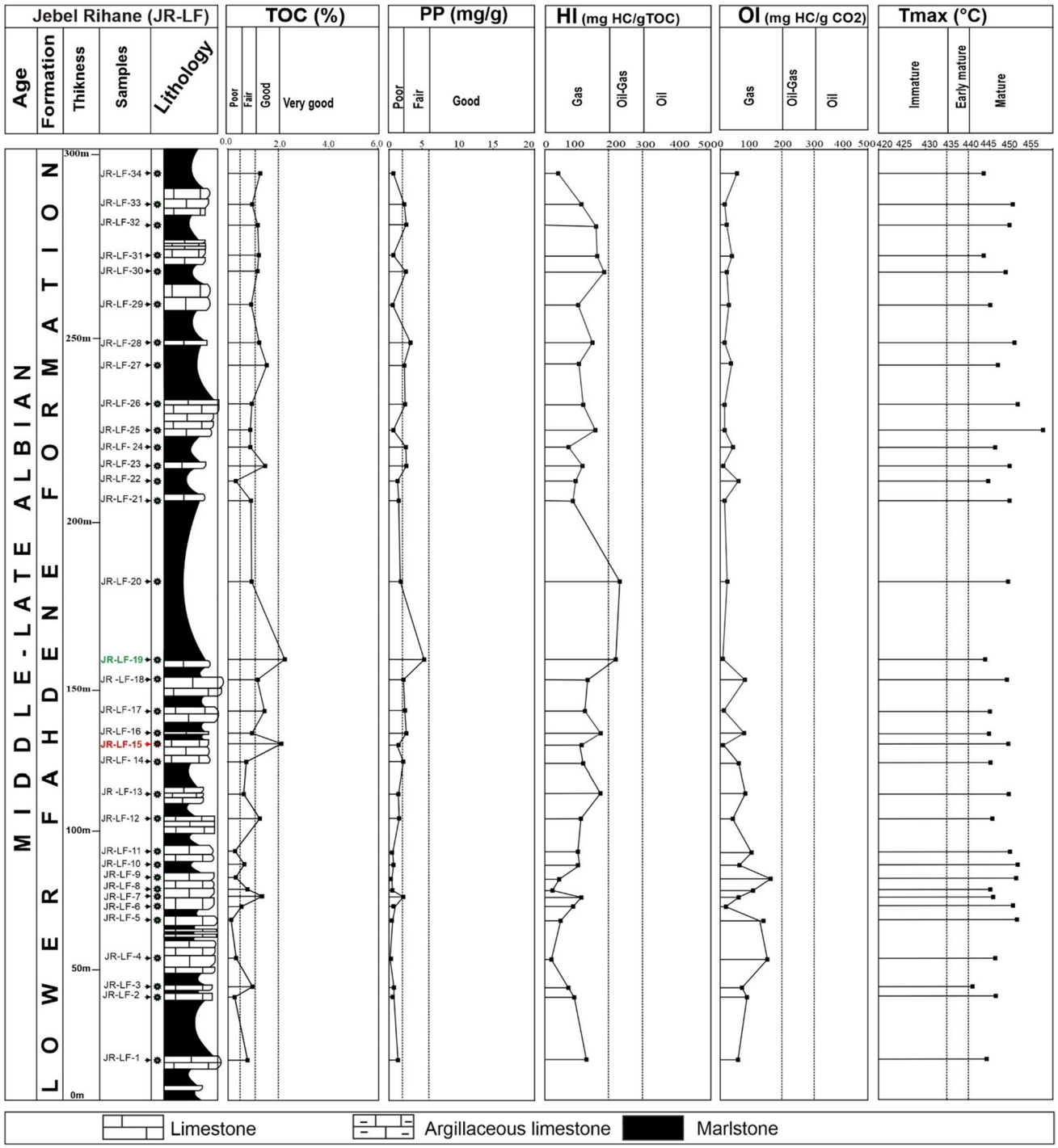

Fig. 6 Geochemical log of the lower Fahdene Formation outcropping at Jebel Rihane

than 1 wt.%. In Jebel Rihane (JR-LF), the TOC contents vary from 0.25 to 1.52 wt.%, 1.06 to 2.06 wt.%, and 0.70 to 2.52 wt.% in the basal, middle, and upper units, respectively.

The lithological column exhibits variable petroleum potential (PP) values ranging from 0.11 to 2.40 mg HC/g rock, 1.96 to 3.36 mg HC/g rock, and 0.55 to 4.87 mg HC/g rock in the basal, middle, and upper units, respectively.

In Oued Siliana section (OS-LF), the TOC contents range from 0.13 to 1.14 wt.% with a mean of 0.49 wt.% (Table 4). The PP is also variable ranging between 0.09 and 5.29 mg HC/g rock, with an average value equal to 1.03 mg HC/g rock.

Toward South-West (sector 2), samples from Lakhaouat locality (LK-LF), have TOC values ranging between 0.58

Table 4 Geochemical parameters recorded from Rock–Eval pyrolysis of the lower Fahdene and Bahloul source rocks

Formation	Age	Section locality		Sample ID	S_1	S_2	PP	TOC	Tmax	HI	OI	PI
Lower Fahdene	Albian	Sector 1	Jebel Rihane(JR-LF)	JR-LF-34	0.14	0.49	0.63	1.14	443	50	54	0.23
				JR-LF-33	0.78	1.30	2.08	0.93	450	140	10	0.37
				JR-LF-32	0.72	1.96	2.68	1.23	449	159	21	0.27
				JR-LF-31	0.24	0.31	0.55	1.13	443	171	48	0.16
				JR-LF-30	0.89	1.48	2.37	0.81	448	183	30	0.38
				JR-LF-29	0.35	0.64	0.99	1.32	445	120	39	0.18
				JR-LF-28	1.13	1.94	3.07	1.25	452	155	20	0.37
				JR-LF-27	0.50	1.58	2.08	1.57	447	101	43	0.24
				JR-LF-26	0.77	1.35	2.12	0.99	451	136	27	0.36
				JR-LF-25	0.68	1.51	2.19	0.96	456	157	20	0.31
				JR-LF-24	0.20	0.67	0.87	0.96	446	70	50	0.23
				JR-LF-23	0.51	2.07	2.58	1.69	450	122	16	0.20
				JR-LF-22	0.39	0.74	1.13	0.70	445	106	56	0.35
				JR-LF-21	0.38	0.82	1.2	0.97	449	85	29	0.32
				JR-LF-20	0.57	1.67	2.24	1.32	452	127	23	0.25
				JR-LF-19	0.89	3.98	4.87	2.52	459	158	6	0.18
				JR-LF-18	0.34	1.65	1.99	1.06	449	156	23	0.17
				JR-LF-17	0.94	2.42	3.36	1.63	451	148	10	0.28
				JR-LF-16	0.35	1.61	1.96	2.06	448	78	22	0.48
				JR-LF-15	0.74	0.99	1.73	0.69	447	143	13	0.04
				JR-LF-14	1.30	1.10	2.40	0.74	445	148	58	0.05
				JR-LF-13	0.73	1.01	1.74	0.64	448	158	73	0.04
				JR-LF-12	0.09	1.67	1.76	1.10	446	151	49	0.05
				JR-LF-11	0.08	0.32	0.40	0.27	449	119	104	0.02
				JR-LF-10	0.04	0.81	0.85	0.75	452	108	61	0.05
				JR-LF-9	0.01	0.13	0.14	0.25	451	52	220	0.07
				JR-LF-8	0.01	0.25	0.26	0.58	445	43	134	0.03
				JR-LF-7	0.02	2.04	2.06	1.52	446	134	67	0.01
				JR-LF-6	0.15	0.57	0.72	0.60	450	95	37	0.02
				JR-LF-5	0.02	0.17	0.19	0.28	452	61	193	0.11
				JR-LF-4	0.01	0.10	0.11	0.32	446	31	206	0.01
				JR-LF-3	0.04	0.74	0.78	1.00	441	74	70	0.05
				JR-LF-2	0.24	0.42	0.66	0.42	446	100	88	0.04
				JR-LF-1	0.36	1.30	1.66	0.78	444	167	60	0.02
				Average	0.44	1.15	1.59	1.00	447	116	58	0.17
			Oued Siliana (OS-LF)	OS-LF-13	0.08	0.80	0.88	0.57	449	140	74	0.09
				OS-LF-12	0.14	0.50	0.64	0.50	450	100	58	0.22
				OS-LF-11	0.38	1.11	1.49	0.68	454	163	29	0.25
				OS-LF-10	0.07	0.18	0.25	0.15	445	120	173	0.27

Table 4 (continued)

Formation	Age	Section locality		Sample ID	S_1	S_2	PP	TOC	Tmax	HI	OI	PI
				OS-LF-9	0.09	0.40	0.49	0.44	452	91	48	0.19
				OS-LF-8	0.06	0.20	0.26	0.21	448	95	90	0.22
				OS-LF-7	0.03	0.13	0.16	0.15	445	87	153	0.21
				OS-LF-6	0.01	0.08	0.09	0.13	446	62	100	0.08
				OS-LF-5	0.06	0.31	0.37	0.34	448	91	50	0.17
				OS-LF-4	0.42	3.02	3.44	1.14	452	265	20	0.12
				OS-LF-3	0.21	2.63	2.84	1.12	445	235	38	0.07
				OS-LF-2	0.16	1.23	1.39	0.60	444	205	57	0.12
				OS-LF-1	0.25	0.86	1.11	0.37	448	232	43	0.22
				Average	0.15	0.88	1.03	0.49	448	145	72	0.17
		Sector 2	Lakhaouat (LK-LF)	LK-LF-5	0.06	2.55	2.61	0.66	429	386	38	0.02
				LK-LF-4	0.04	3.72	3.76	1.86	434	200	57	0.01
				LK-LF-3	0.06	5.04	5.10	1.35	428	373	40	0.01
				LK-LF-2	0.03	1.55	1.58	0.58	432	267	71	0.02
				LK-LF-1	0.03	1.03	1.06	0.67	439	154	106	0.02
				Average	0.04	2.78	2.82	1.02	432	276	62	0.02
Bahloul	Late Cenom.-earlyTuronian	Sector 1	Oued Siliana (OS-BH)	OS-BH-52	0.49	3.01	3.5	1.84	439	164	41	0.14
				OS-BH-51	0.09	0.36	0.45	0.18	443	200	339	0.20
				OS-BH-49	0.39	2.81	3.20	1.47	442	191	67	0.12
				OS-BH-48	0.14	1.68	1.82	1.3	444	129	75	0.08
				OS-BH-47	0.46	3.78	4.24	1.87	441	202	63	0.11
				OS-BH-46	0.13	1.40	1.53	0.63	442	222	71	0.08
				OS-BH-45	0.18	1.82	2.00	0.70	441	260	111	0.09
				OS-BH-44	0.19	2.08	2.27	0.49	437	221	135	0.08
				OS-BH-43	0.33	3.67	4.00	1.49	442	246	38	0.08
				OS-BH-42	0.45	6.13	6.58	2.31	441	265	29	0.07
				OS-BH-41	0.57	7.31	7.88	2.63	442	278	30	0.07
				OS-BH-40	0.47	4.63	5.10	1.31	444	353	17	0.09
				OS-BH-39	0.39	6.30	6.69	2.19	442	288	22	0.06
				OS-BH-38	0.52	6.74	7.26	2.40	442	281	8	0.07
				OS-BH-37	0.49	6.23	6.72	2.24	441	278	14	0.07
				OS-BH-36	0.57	8.55	9.12	2.8	444	305	29	0.06
				OS-BH-35	0.21	4.65	4.86	2.03	441	229	75	0.04
				OS-BH-34	0.39	4.34	4.73	1.69	444	257	45	0.08
				OS-BH-33	0.49	6.47	6.96	2.20	445	294	32	0.07
				OS-BH-32	0.32	4.44	4.76	2.04	442	218	50	0.07
				OS-BH-31	0.34	3.72	4.06	1.35	443	276	47	0.08
				OS-BH-30	0.65	5.74	6.39	2.27	441	253	37	0.04
				OS-BH-29	0.28	2.38	2.66	1.05	442	227	61	0.02
				OS-BH-28	0.35	3.51	3.86	1.26	441	279	60	0.04
				OS-BH-27	0.08	2.53	2.61	1.42	441	178	80	0.13

Table 4 (continued)

Formation	Age	Section locality		Sample ID	S_1	S_2	PP	TOC	Tmax	HI	OI	PI
				OS-BH-26	0.21	2.81	3.02	1.46	439	192	59	0.07
				OS-BH-25	0.03	1.47	1.5	1.37	439	107	91	0.03
				OS-BH-24	0.18	1.75	1.93	1.09	441	161	75	0.03
				OS-BH-23	0.33	4.50	4.83	1.93	441	233	46	0.03
				OS-BH-21	0.28	11.68	11.96	4.10	440	285	40	0.09
				OS-BH-20	0.87	17.74	18.61	5.13	445	346	7	0.09
				OS-BH-19	0.58	10.00	10.58	3.73	442	268	39	0.17
				OS-BH-18	0.27	7.49	7.76	4.10	443	183	53	0.07
				OS-BH-17	0.41	9.17	9.58	4.24	442	216	26	0.23
				OS-BH-16	0.07	2.34	2.41	1.93	442	137	61	0.04
				OS-BH-15	0.15	4.09	4.24	2.58	441	159	50	0.07
				OS-BH-14	0.06	3.15	3.21	2.51	441	125	49	0.02
				OS-BH-13	0.38	7.88	8.26	3.19	442	247	29	0.06
				OS-BH-12	0.19	5.77	5.96	3.56	441	162	52	0.03
				OS-BH-11	0.14	2.50	2.64	1.18	443	212	84	0.08
				OS-BH-10	0.56	10.98	11.54	4.37	442	251	14	0.04
				OS-BH-9	0.26	5.00	5.26	2.06	441	243	10	0.03
				OS-BH-8	0.16	6.24	6.40	2.21	443	282	85	0.03
				OS-BH-7	0.27	5.88	6.15	2.40	442	245	20	0.03
				OS-BH-6	0.33	13.86	14.19	4.39	439	316	15	0.07
				OS-BH-5	0.08	2.45	2.53	1.39	442	176	43	0.02
				OS-BH-4	0.14	2.02	2.16	1.39	442	145	42	0.02
				OS-BH-3	0.23	3.17	3.40	2.11	441	150	45	0.05
				OS-BH-2	0.75	1.91	2.66	1.24	440	154	44	0.17
				Average	0.32	5.07	5.40	2.12	441	228	55	0.07
			Kenana (KN-BH)	KN-BH-15	0.18	5.68	5.86	3.81	440	149	66	0.03
				KN-BH-14	0.30	9.53	9.83	3.42	436	279	50	0.03
				KN-BH-13	1.00	24.09	25.09	5.25	434	459	27	0.04
				KN-BH-12	0.36	4.29	4.65	1.07	438	401	54	0.08
				KN-BH-11	1.61	27.83	29.44	6.44	438	432	17	0.05
				KN-BH-9	0.37	4.16	4.53	1.66	438	251	27	0.08
				KN-BH-8	0.53	6.62	7.15	2.00	438	331	31	0.07
				KN-BH-7	0.71	6.98	7.69	2.21	440	316	18	0.09
				KN-BH-6	0.48	4.02	4.50	2.26	437	178	18	0.11
				KN-BH-5	0.56	8.48	9.04	2.25	439	377	26	0.06
				KN-BH-4	0.58	9.24	9.82	2.53	439	365	44	0.06
				KN-BH-3	0.37	4.82	5.19	1.65	438	292	35	0.07
				KN-BH-2	0.32	4.02	4.34	1.74	440	231	14	0.07
				Average	0.57	9.32	9.89	2.85	438	310	32	0.06
		Sector 2	Oued Merir (OMR-BH)	OMR-BH-9	0.47	26.33	26.8	4.04	419	652	27	0.02
				OMR-BH-8	0.19	19.72	19.91	2.83	422	697	31	0.01
				OMR-BH-7	0.09	12.75	12.84	2.12	426	601	49	0.01
				OMR-BH-6	1.21	41.95	43.16	5.77	423	727	23	0.03
				OMR-BH-5	2.15	51.56	53.71	6.97	421	740	17	0.04

Table 4 (continued)

Formation	Age	Section locality	Sample ID	S_1	S_2	PP	TOC	Tmax	HI	OI	PI
			OMR-BH-4	2.16	53.71	55.87	8.06	421	666	27	0.04
			OMR-BH-3	0.55	31.99	32.54	4.78	420	669	32	0.02
			OMR-BH-2	2.72	64.71	67.43	8.61	421	752	13	0.04
			OMR-BH-1	0.04	2.23	2.27	1.1	438	203	151	0.02
			Average	1.07	33.87	34.94	4.92	423	634	41	0.03
		Lakhaouat (LK-BH)	LKWF-BH-5	0.61	20.75	21.36	3.16	423	657	25	0.03
			LKWF-BH-3	2.19	41.32	43.51	6.01	423	688	12	0.05
			LKWF-BH-2	2.38	33.77	36.15	4.87	423	693	13	0.07
			LKWF-BH-1	0.73	20.00	20.73	2.58	426	775	10	0.04
			Average	1.48	28.96	30.44	4.15	424	703	15	0.05
		Lakhaouat Mine Borehole (LKM-BH)	LKM-BH-4	0.70	11.65	12.35	2.78	432	419	15	0.06
			LKM-BH-3	0.50	8.06	8.56	2.15	429	375	14	0.06
			LKM-BH-2	0.66	12.55	13.21	3.15	430	398	24	0.05
			LKM-BH-1	2.04	32.44	34.48	6.86	432	473	13	0.06
			Average	0.97	16.18	17.15	3.74	431	416	16	0.06

S_1 Free hydrocarbon; S_2 Potential hydrocarbon; *PP* (S_1+S_2) Petroleum potential; *TOC* Total organic carbon; $T_{max,}$ Temperature at the peak of S_2; *HI* Hydrogen index (S_2/TOC*100); *OI* Oxygen index (S_3/TOC*100) and *PI* Production index (S_1/(S_1+S_2)

and 1.86 wt.% with a mean of 1.02 wt.% (Table 4). The PP values vary from 1.06 to 5.10 with a mean of 2.82 mg of HC/g TOC.

In the two investigated cross-sections of sector 1, the Fahdene OM shows HI, OI, and T_{max} values ranging between 31 and 265 mg HC/g TOC, 6 and 220 mg CO_2/g TOC, and 471 and 459 °C respectively.

In sector 2, the Lakhaouat locality shows HI values ranging from 154 to 386 mg HC/g TOC, with OI and T_{max} values in the range of 38–106 mg CO_2/g TOC and 429–439 °C, respectively (Table 4).

Bahloul Fm

The TOC contents and Rock–Eval pyrolysis results of the Bahloul samples are shown in Table 4 and Fig. 7. The stratigraphic distribution of the TOC contents throughout the Oued Siliana section (OS-BH) in sector 1 (Fig. 7) shows maximum values at the base of the lower unit (U_1) up to 5.13 wt.% TOC. However, in the middle (U_2) and the upper (U3) units, TOC values are in the range of 1.05 to 2.27 wt.% and 0.18 to 2.63 wt.%, respectively.

The PP varies from 1.5 to 18.61 mg HC/g rock in unit1 (U1), 2.61 to 6.39 mg HC/g rock, and 0.45 to 9.12 mg HC/g rock in unit 2 (U2) and unit 3 (U3), respectively.

In Kenana section (KN-BH) of sector 1, the TOC values vary from 1.07 to 6.44 wt.% (Table 4). The PP ranges between 4.34 and 29.44 mg HC/g rock with a mean of 9.89 mg HC/g rock.

In sector 2, the samples collected from Oued Merir (OMR-BH), display variable TOC contents ranging between 1.1 and 8.61 wt. % with a mean of 4.92 wt.%. Their PP values range between 2.27 and 67.43 mg HC/g rock.

In Lakhaouat section and Lakhaouat mine, the TOC contents range from 2.58 to 6.01 wt.% and from 2.15 to 6.86 wt. %, respectively. The PP values vary between 20.73 and 43.51 mg HC/g rock in Lakhaouat section and from 8.56 to 34.48 mg HC/g rock in Lakhaouat mine.

In the two investigated cross-sections of sector 1, the OM preserved in the Bahloul Fm of Oued Siliana (OS-BH) and Kenana (KN-BH) is characterized by HI values in the range of 107–459 mg HC/g TOC with OI values between 7 and 91 mg CO_2/g TOC, and average T_{max} values of 438 °C in Kenana and 441 °C in Oued Siliana.

In sector 2, samples collected from Oued Merir (OMR-BH), Lakhaouat section (LKWF-BH), and Lakhaouat mine (LKM-BH), the HI, OI, and T_{max} values are in the range of 203–775 mg HC/g TOC, 10–151 mg CO_2/g TOC, and 419–438 °C, respectively (Table 4).

Molecular geochemistry

Source rock bitumen

Three extracted source rock samples from Fahdene Fm (two samples: JR-LF9 and OS-LF4 from sector 1 and one sample: LK-LF5 from sector 2), as well as three extracts from

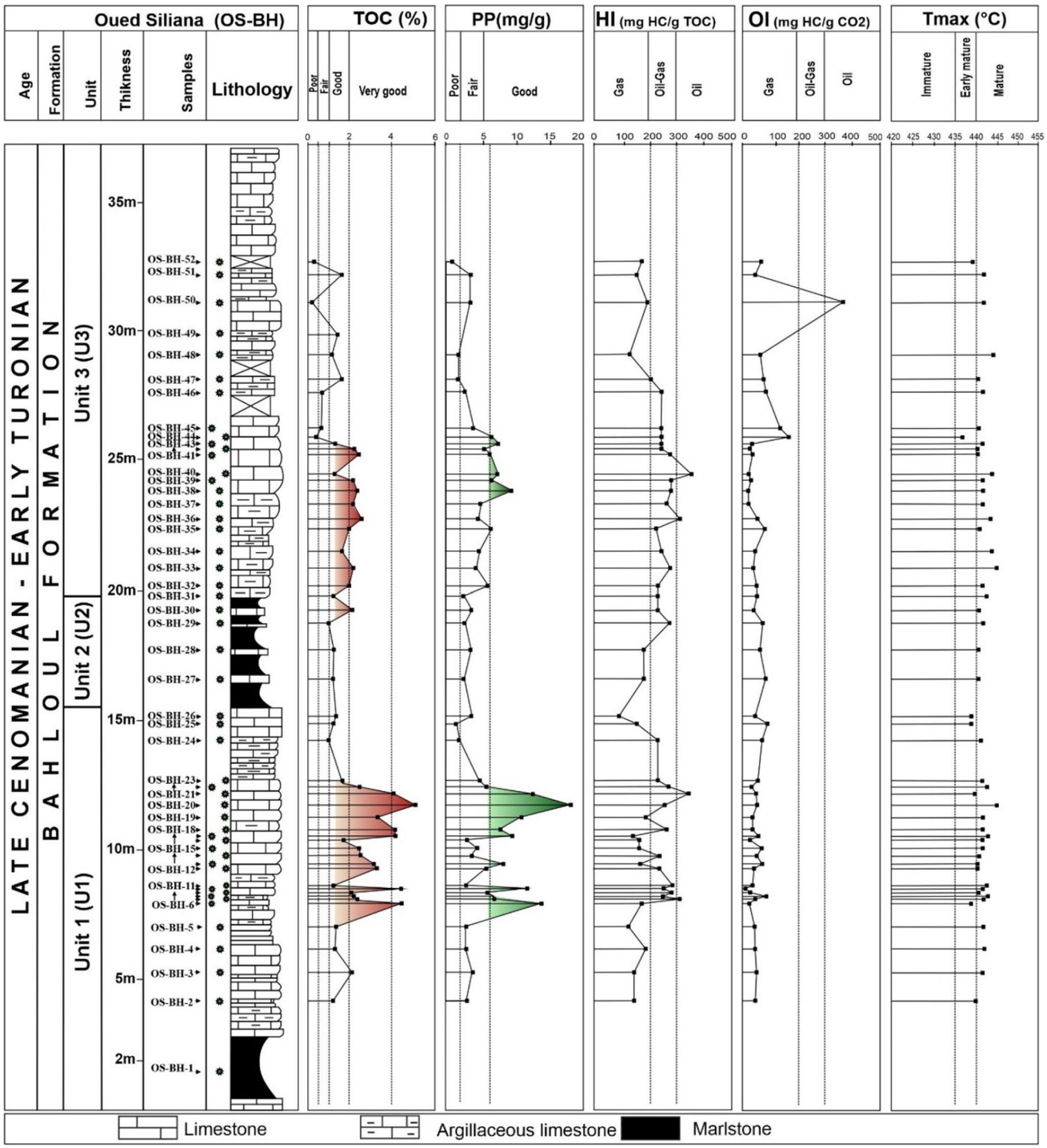

Fig. 7 Geochemical log of the Bahloul Formation outcropping at Oued Siliana (Saidi 2003)

Bahloul Fm (OS-BH33 from sector 1 and LKM-BH2, and OMR-BH3 from sector 2), were analyzed (Fig. 8).

In general, *n*-alkanes exhibit a unimodal distribution ranging from *n*-C_{11} to *n*-C_{35} with a dominance of short-chain compounds around *n*-C_{17} (Fig. 8). Pristane (Pr) and phytane (Ph) are present but less abundant than the adjacent *n*-C_{17} and n-C_{18} alkanes, resulting in low Pr/*n*-C_{17} and Ph/*n*-C_{18} ratios < 1 (Fig. 8; Table 5). Pr/Ph ratios range from 1.34 to 2.09 and from 0.46 to 0.95 for lower Fahdene and Bahloul samples, respectively (Fig. 8; Table 5). The degree of waxiness is between 0.28–0.82 and 0.20–0.36 in lower Fahdene and Bahloul source rock extracts, respectively (Table 5).

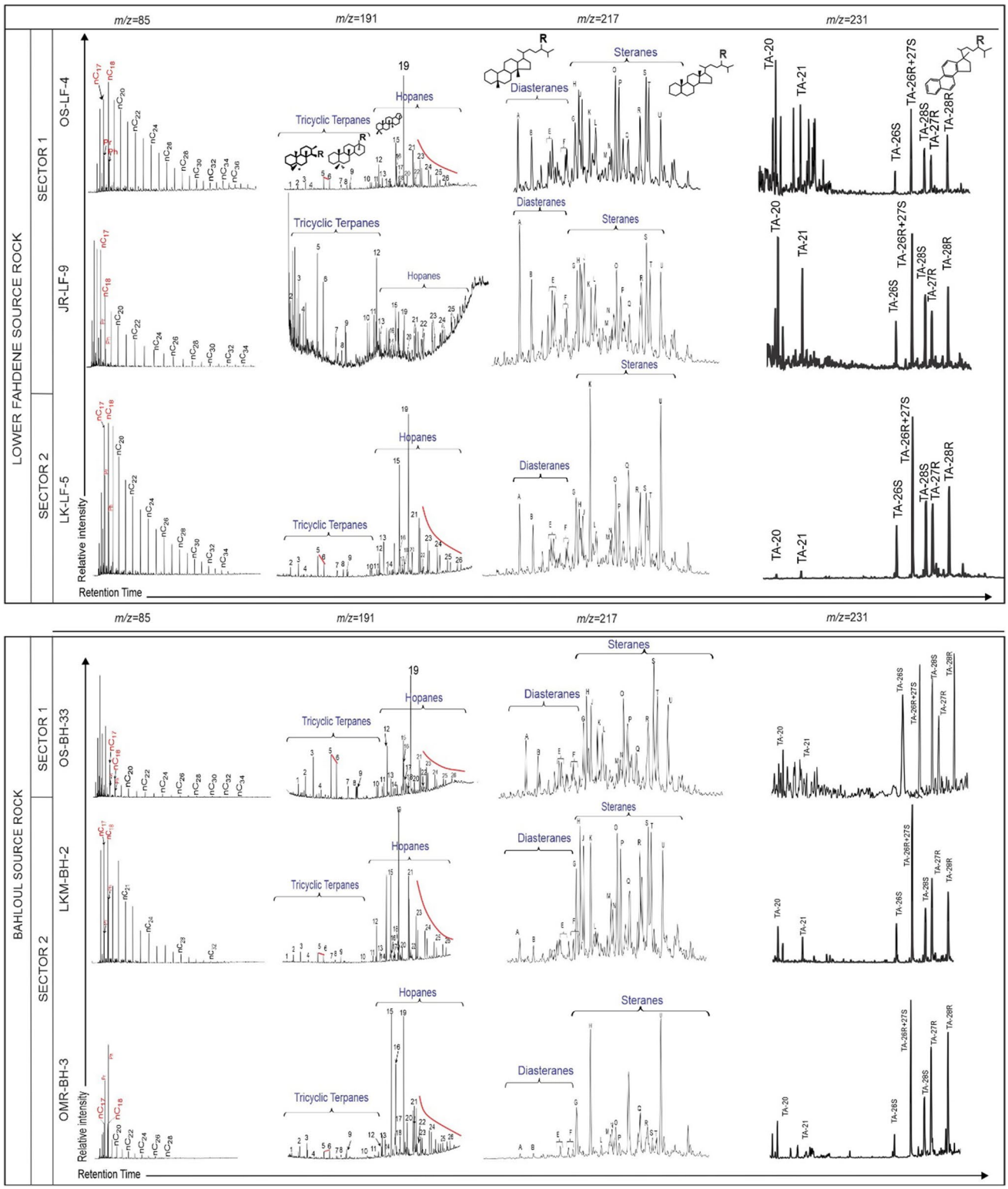

Fig. 8 Mass chromatograms showing the distribution of aliphatic fraction (*m/z* 85), terpanes (*m/z* 191), steranes (*m/z* 217), and tri-aromatics (*m/z* 231) of the lower Fahdene and the Bahloul source rocks from sectors 1 and 2 (for key, see Table 3)

Table 5 Biomarkers parameters of oil seeps (OS1-10) and bitumen from source rock samples

Biomarkers	OS1	OS2	OS3	OS4	OS5	OS6	OS7	OS8	OS9	OS10	OS-LF4	JR-LF9	LK-LF-5	OS-BH-33	LKM-BH	OMR-BH-3
CPI	1.05	1.04	1.18	1.11	0.89	1.12	0.99	1.05	1.07	0.97	0.98	1.04	0.80	1.01	1.28	0.47
Degree of waxiness	0.53	0.77	2.42	1.99	0.39	0.53	0.63	0.84	0.43	0.55	0.82	0.28	0.64	0.31	0.36	0.20
Pr/nC_{17}	1.00	0.73	0.56	0.20	0.73	0.59	0.39	0.67	0.72	0.49	0.31	0.31	0.67	0.35	0.25	2.25
Ph/nC_{18}	1.01	0.56	0.45	0.28	1.52	0.46	0.34	0.62	0.51	0.52	0.27	0.25	0.41	0.18	0.52	3.98
Pr/Ph	1.35	1.34	1.00	0.18	0.75	1.57	1.75	1.21	0.59	0.56	1.34	2.09	1.56	0.95	0.46	0.67
C_{19}/C_{23}	0.16	0.27	0.21	0.22	0.66	0.15	0.16	0.18	0.10	0.17	0.11	0.35	0.44	0.28	0.66	0.88
C_{22}/C_{21}	0.23	0.19	0.56	0.30	0.17	0.48	0.23	0.23	0.21	0.23	0.24	0.23	0.17	0.11	0.21	0.12
C_{26}/C_{25}	1.00	0.85	0.93	0.89	0.73	0.48	0.86	0.79	1.02	0.88	2.58	1.38	1.16	0.95	0.74	0.58
$C_{23}/C_{30}H$	0.11	0.34	0.12	0.13	0.05	0.40	0.14	0.16	0.66	0.11	0.13	2.19	0.13	0.37	0.07	0.05
Ts/(Tm + Ts)	0.64	0.68	0.67	0.66	0.20	0.57	0.52	0.53	0.56	0.44	0.56	0.55	0.41	0.74	0.80	0.38
Ts/Tm	1.79	2.10	2.03	1.96	0.35	1.30	1.10	1.11	0.62	1.13	1.28	1.21	0.68	2.81	4.01	0.61
$C_{29}/C_{30}H$	0.45	0.51	0.59	0.49	0.47	0.81	0.63	0.65	0.72	0.68	0.38	0.65	0.68	0.46	0.40	0.66
m_{30}/H_{30}	0.11	0.12	0.10	0.10	0.07	0.10	0.10	0.11	0.22	0.12	0.10	0.18	0.13	0.10	0.08	0.23
$G/(G + H_{30})$	0.04	0.05	0.07	0.06	0.06	0.10	0.05	0.05	0.13	0.02	0.07	0.15	0.04	0.05	0.06	0.08
$C_{32}S/R + S$	0.57	0.59	0.49	0.58	0.61	0.63	0.61	0.59	0.61	0.64	0.58	0.40	0.59	0.58	0.60	0.55
C_{35}/C_{34}	0.55	0.54	0.68	0.72	0.79	0.68	0.64	0.59	1.00	0.68	0.78	0.56	0.67	0.89	0.77	0.97
$C_{35}/(C_{31}\text{-}C_{35})$	0.06	0.05	0.08	0.07	0.06	0.06	0.07	0.06	0.09	0.07	0.08	0.17	0.06	0.08	0.07	0.09
$C_{24}Tet/C_{26}$	0.52	0.62	0.78	0.79	1.23	0.85	0.42	0.77	0.53	0.57	0.68	0.22	0.48	0.44	1.66	1.04
$C_{24}Tet/(C_{24}Tet + C_{23}tr)$	0.25	0.18	0.41	0.28	0.34	0.28	0.24	0.31	0.25	0.28	0.38	0.24	0.26	0.21	0.41	0.21
$C_{29}H/C_{29}H + C_{29}M$	0.88	0.91	0.92	0.90	0.93	0.82	0.92	0.91	0.76	0.92	0.71	0.70	0.88	0.83	0.99	0.61
$C_{30}H/C_{30} + C_{30}M$	0.89	0.89	0..91	0.90	0.93	0.90	0.90	0.90	0.82	0.89	0.91	0.85	0.88	0.91	0.92	0.81
$C_{27}\beta\alpha S/C_{27}\alpha\alpha S$	0.75	1.76	0.57	1.65	0.20	1.16	0.99	1.80	1.9	0.75	1.00	1.90	1.56	0.78	0.26	0.49
$C_{29}\alpha\alpha R/C_{27}\alpha\alpha R$	1.03	0.96	1.33	0.99	1.22	1.86	1.81	1.10	0.88	0.91	1.04	0.84	2.32	1.30	1.08	0.93
$C_{29}\alpha\ \beta\beta/(\alpha\beta\beta + \alpha\alpha\alpha)$	0.50	0.52	0.57	0.52	0.57	0.46	0.57	0.53	0.46	0.41	0.60	0.63	0.37	0.59	0.58	0.16
$C_{29}\alpha\alpha\alpha 20S$ / (20S + 20R)	0.36	0.49	0.54	0.43	0.46	0.58	0.69	0.58	0.42	0.41	0.51	0.53	0.31	0.43	0.37	0.42
$C_{29}\beta\beta R/\ C_{29}\alpha\alpha R$	0.95	1.12	1.49	0.98	1.22	1.12	2.22	1.36	0.79	0.59	1.68	0.67	0.55	1.47	2.85	0.79
C_{27}Sterane (%)	43	37	34	35	33	34	27	29	44	37	33	37	35	37	37	35
C_{28}Sterane (%)	31	24	31	26	28	34	26	28	21	23	29	22	27	19	29	28
C_{29}Sterane (%)	26	39	35	39	39	32	47	43	36	40	38	40	38	44	34	37
$C_{27}\beta\alpha(R + S)/C_{27}\alpha\alpha(R + S)$	0.58	1.39	1.24	1.15	0.17	1.23	0.81	1.80	2.84	0.48	1.02	2.69	1.57	0.70	0.20	0.49
TAS	0.15	0.22	0.37	0.22	0.07	0.16	0.19	0.32	0.03	0.01	0.83	0.80	0.06	0.15	0.14	0.08
C_{26}/C_{28}TA(20S)	0.64	0.61	0.63	0.70	0.70	0.24	0.41	0.23	0.68	0.53	0.50	0.60	0.30	0.88	0.73	0.38
$C_{20}TA/(C_{20} + C_{28}R)TA$	0.33	0.45	0.62	0.47	0.19	0.10	0.34	0.94	0.05	0.01	0.69	0.58	0.25	0.26	0.33	0.23

CPI, carbon preference index = 1/2(($C_{25} + C_{27} + C_{29+}\ C_{31+}\ C_{33}$)/($C_{24} + C_{26} + C_{28} + C_{30} + C_{32}$) + ($C_{25} + C_{27} + C_{29+}\ C_{31+}\ C_{33}$)/($C_{26} + C_{28} + C_{30} + C_{32+}\ C_{34}$))(Peters, 2005), degree of waxiness = ($\sum C_{21}\text{-}C_{31}/\sum C_{15}\text{-}C_{20}$), Pr: Pristane, Ph: Phytane, Ts/Tm: 18α(H)-22,29,30-trisnorneohopane (C_{27}Ts)/17α(H)-22,29,30-trisnorhopane (C_{27}Tm), C_{19}/C_{23}:TricyclicTerpane C_{19}/ Tricyclic Terpane $C_{23,}\ C_{24}$ Tet/(C_{24} Tet + C_{23}: Tetracyclic Terpane C_{24}/ Tetracyclic Terpane + C_{23}Tricyclic Terpane, $Ga/(Ga + H_{30})$: Gammacerane/ Gammacerane + $C_{30}\alpha\beta$hopane, m_{30}/H_{30}:moretane/ hopane, $C_{35}/(C_{31}\text{-}C3_{5})$: Homohopane index: C_{35} (R + S)/total homohopanes C_{31}- C_{35} (R + S), %C_{27} steranes: $C_{27}/(C_{27} + C_{28} + C_{29})$ steranes; %C_{28} steranes: $C_{28}/(C_{27} + C_{28} + C_{29})$ steranes;%C_{29} steranes: $C_{29}/(C_{27} + C_{28} + C_{29})$ steranes; C27βα(R + S)/C27αα(R + S) = C27diasterane/C27 regular sterane, TAS-Triaromatic steroids = ($C_{21} + C_{22}$)/($C_{20} + C_{21} + C_{26} + C_{27} + C_{28}$

The analysis of terpanes biomarkers (*m/z* 191) shows that C_{19}- to C_{25}-tricyclic terpanes are present in samples from the two sectors (Fig. 8) but their abundance is generally low as indicated by the low $C_{23}tr/C_{30}H$ ratios ranging from 0.05 to 0.37 in the Bahloul Fm and 0.13 in the lower Fahdene Fm (excepting JR-LF-9 sample in sector 1: 2.19). C_{23} is the most abundant tricyclic terpane and $C_{19}tr/C_{23}tr$ ratios are generally lower than 1.0 (0.11–0.44 and 0.28–0.88 for the lower Fahdene and Bahloul extracts, respectively). The $C_{22}tr/C_{21}tr$ and $C_{26}tr/C_{25}tr$ tricyclic terpane ratios for the lower Fahdene samples are 0.17–0.24 and 1.16–2.58, respectively, while for the Bahloul Fm samples they range from 0.11 to 0.21 and 0.58 to 0.95, respectively.

Complete C_{27} to C_{35}-17α(H), 21β(H)-hopane series were detected in all samples (Fig. 8). The regular 17α(H), 21β(H)-hopane ($C_{30}H$) is the most abundant pentacyclic terpane in all the source rock extracts. C_{29}-αβ/C_{30}-αβ ratios vary, in general, from 0.38 to 0.68 in the lower Fahdene Fm and from 0.40 to 0.66 in the Bahloul Fm. The gammacerane (G) was detected in all samples in low to very low concentrations compared to C_{30}-αβ hopanes ($G/(G+C_{30}H)$ ratio < 0.13). Extended hopanes or homohopanes are dominated by C_{31}-homohopane ($C_{31}HH$) and generally decrease toward the C_{35}-homohopane ($C_{35}HH$) (Fig. 8). The homohopane ($C_{31}HH$-$C_{35}HH$) distribution exhibits relatively low $C_{35}HH/C_{34}HH$ values ranging between 0.56 and 0.78 in the lower Fahdene and between 0.77 and 0.97 in the Bahloul samples (Table 5).

The C_{27}, C_{28}, and C_{29} steranes have similar distributions ($C_{29} > C_{27} > C_{28}$) in samples of the lower Fahdene and Bahloul Fms from different sections, except sample LKM-BH-2 in sector 2 which shows a slight predominance of C_{27} (37%) over the C_{29} (34%) and C_{28} (29%) homologous (Table 5). Relative abundances of C_{27}, C_{28}, and C_{29} regular steranes of the lower Fahdene Fm range between 33 and 37%, 22 and 29%, and 38 and 40% respectively, and those of the Bahloul bitumen range between 35 and 37%, 19 and 28%, and 34 and 44%, respectively (Table 5).

The diasteranes content of the lower Fahdene bitumen is fair to high ($C_{27}βα/C_{27}αα$ range: 1.02–2.69), unlike that recorded in the Bahloul samples which are low to fair (0.20–0.70). C_{30}-sterane was recorded in small quantities in analyzed source rock bitumen (Table 5). The distribution ranges of C_{29}-steranes 20S/(20S + 20R) and αββ/(αββ + ααα) in the lower Fahdene extracts vary between 0.37–0.63 and 0.16–0.59, respectively, and 0.37–0.43 and 0.16–0.69 in the Bahloul extracts, respectively.

The analyzed biomarker maturity parameters show the high C_{29}20S/(20S + 20R)(0.51–0.53) and ββ/(ββ + αα) (0.59–0.60) sterane ratios in the lower Fahdene samples of Oued Siliana (OS-LF4) and Jebel Rihane (JR-LF9), respectively, in sector 1 (Table 5). However, in sector 2 of Jebel Ech-Cheid, the lower Fahdene of Lakhaouat section (LK-LF5) exhibits low 20S/(20S + 20R) and ββ/(ββ + αα) C29 sterane ratios (0.31 and 0.37, respectively) (Table 5). Likewise, the Bahloul samples outcropping in the Oued Merir (OMR-BH3, sector 2) section exhibit the lower 20S/(20S + 20R) sterane (in the order of 0.42) and ββ/(ββ + αα) C29 sterane ratios (in the order of 0.16). Conversely, in sector 1, the Oued Siliana (OS-BH33) section exhibits the high 20S/(20S + 20R) sterane (in the order of 0.43) and ββ/(ββ + αα) C_{29} sterane (0.59) ratios.

The *m/z* 231 mass-chromatograms show the distribution of triaromatic steroids (TAS) in the lower Fahdene and Bahloul bitumen (Fig. 8) ranging between 0.06 and 0.83 in the lower Fahdene Fm and 0.08 to 0.15 in the Bahloul Fm (Table 5) (Peters et al. 2005).

In sector 1, samples of lower Fahdene and Bahloul Fms are characterized by high TAS values (0.80–0.83 and 0.14–0.15, respectively), while in sector 2 they are low (0.06 and 0.08, respectively).

The distributions of triaromatic steroids are characterized by a relatively high abundance of C_{26}20R + C_{27}20S, C_{28}20S, and C_{28}20R triaromatic steroids, while C_{26}20S occurs as least (Fig. 8). Samples OS-LF-4 and JR-LF-9 in sector 1 reveal the predominance of C_{20} and C_{21} TAS peaks over higher homologous, while C_{26} 20R + C_{27} 20S are predominant in all samples except sample OS-BH-33 in sector 1 which C_{26} compounds occur in relatively low abundance (Fig. 8). Ratios of C_{26}-/C_{28}-TA (20S) and C_{20}-TA/(C_{20} + C_{28}R)-TA in the lower Fahdene and Bahloul samples are 0.50, 0.60, and 0.88 and 0.58, 0.69, and 0.33, respectively, in sector 1, while values decreased in sector 2 (in the order of 0.30–0.38 and 0.23, respectively) (Peters et al. 2005).

Oil seeps and bitumen impregnations

The mass chromatograms *m/z* 85 of OS1 and OS2 samples from sector 1 show a unimodal *n*-alkanes distribution ranging between *n*-C_{12} and *n*-C_{34} + and maximizing at *n*-C_{16} and *n*-C_{18} excepting the OS3 sample from sector 1 which shows a bimodal distribution of *n*-alkanes that maximizes at *n*-C_{25} (Fig. 9). The studied oil seep samples are characterized by relatively high abundance of *n*-C_{15} to *n*-C_{20} alkanes in the saturate fraction as indicated by the low degree of waxiness (0.53–0.77). However, the degree of waxiness in the OS3 sample is relatively high (2.42) (Table 5). The samples from sector 1 have no clear odd/oven carbon number predominance with CPI ranging from 1.04 to 1.18. The Pr/Ph ratio values are relatively fair (between 1.00 and 1.35) (Peters et al. 2005).

The OS4, OS5, OS6, and OS8 samples from sector 2 show a unimodal *n*-alkanes distribution ranging between *n*-C_{12} and *n*-C_{34} + with a maximum at *n*-C_{16} and *n*-C_{18} excepting OS7 from sector 2 which shows a bimodal

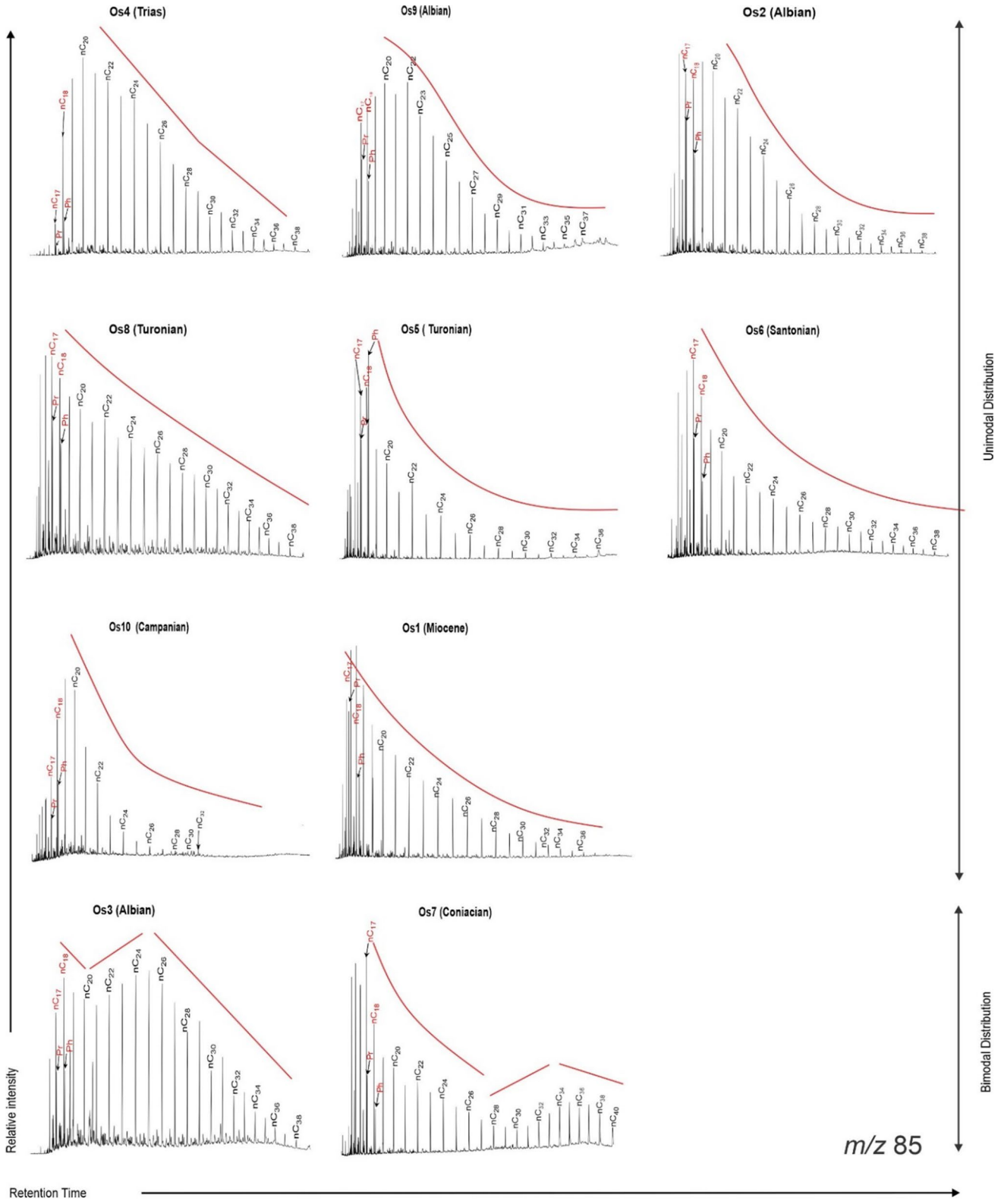

Fig. 9 Mass chromatograms (*m/z* 85) of the aliphatic fractions showing the *n*-alkanes and acyclic isoprenoids distribution of the selected oil seep samples (for key, see Table 3)

distribution of *n*-alkanes maximizing at *n*-C_{25} (Fig. 9). The samples OS5, OS6, OS7, and OS8 are characterized by relatively high abundance of *n*-C_{15} to *n*-C_{20} alkanes and the low degree of waxiness (0.39–0.84) in the saturate fraction. The degree of waxiness in the OS4 sample is relatively high (1.99) (Table 5). The CPI of samples from sector 2 ranges from 0.99 to 1.12. The Pr/Ph ratio values are high (between 1.21 and 1.75) with the exception of OS4 and OS5 samples characterized by low values of Pr/Ph ratios in the order of 0.18 (< 1).

The OS9 and OS10 samples from sector 3 show a unimodal *n*-alkanes distribution ranging between *n*-C_{12} and *n*-C_{34} + and maximizing at *n*-C_{16} and *n*-C_{18} (Fig. 9) with the relatively high abundance of n-C_{15} to n-C_{20} alkanes and the low degree of waxiness (0.43–0.55) in the saturate fraction. The CPI and Pr/Ph ratio values range from 0.97 to 1.07 and between 0.56 and 0.59 (< 1), respectively.

The values of Pr/*n*-C_{17} and Ph/*n*-C_{18} ratios in sector 1 range between 0.56–1.01 and 0.45–1.01, respectively (Table 5), while ratio values range between 0.20–0.67 and 0.28–1.52 in sector 2 and between 0.49–0.72 and 0.51–0.52 in sector 3 (Table 5).

The analyzed oil seep samples from sector 1 (OS1, OS2, OS3) have a higher abundance of pentacyclic terpanes than tricyclic terpanes (Fig. 10), with ratios of tricyclic (tr) to pentacyclic terpanes (H) materialized by the dominant peak of tricyclic terpanes is C_{23}tr, showing an ascending trend of $C_{19}tr < C_{20}tr < C_{21}tr < C_{23}tr$. The C_{19}tr/C_{23}tr, and C_{24}Tet/C_{26}tr ratios are low ranging from 0.16 to 0.27 and from 0.52 to 0.78, respectively, while the C_{26}tr/C_{25}tr ratios are relatively high in the range of 0.85–1.00.

The conventional hopane with a carbon number of 30αβH (C_{30}-17α, 21β hopane) is the dominant peak. There are few rearranged hopanes, only a small amount of C_{29}Ts (C_{29}-18α-neohopanes) and an extremely small amount of 30 Diah (C_{30}-17α-diahopanes) that were detected. The gammacerane indice (GI) is low in the analyzed samples (GI = 0.04–0.07). The hopane distribution patterns are characterized by a regular stair-step progression of C_{31} to C_{35} homohopanes (C_{31}HH-C_{35}HH) with the predominance of 22S over 22R epimers. These samples display low to fair C_{35} HH/C_{34} HH (0.55–0.68) and small homohopane indices (C_{35}HH/C_{31}HH-C_{35}HH), ranging between 0.05 and 0.08.

The analyzed samples from sector 2 (OS4, OS5, OS6, OS7, and OS8) have a higher abundance of pentacyclic terpanes than tricyclic terpanes (Fig. 10), with ratios of tricyclic (tr) to pentacyclic terpanes (H) materialized by low C_{23}tr/C_{30}H ratios ranging from 0.05 to 0.40. In almost the analyzed samples, the dominant peak of tricyclic terpanes is C_{23}tr, showing an ascending trend of $C_{19}tr < C_{20}tr < C_{21}tr < C_{23}tr$. The C_{19}tr/C_{23}tr, and C_{24}Tet/C_{26}tr ratios are low, ranging from 0.15 to 0.22 and from 0.42 to 0.85, while the C_{26}tr/C_{25}tr ratios are relatively high in the range of 0.48–0.89 (Table 5).

The conventional hopane with a carbon number of 30αβH (C_{30}-17α, 21β hopane) is the dominant peak in the analyzed samples. There are few rearranged hopanes, only a small amount of C_{29}Ts (C_{29}-18α-neohopanes) and an extremely small amount of 30 Diah (C_{30}-17α-diahopanes) that were detected (Fig. 10). The content of gammacerane is low (GI = 0.05–0.10). The hopane distribution patterns are characterized by a regular stair-step progression of C_{31} to C_{35} homohopanes (C_{31}HH-C_{35}HH) with the predominance of 22S over 22R epimers. These samples display low to fair C_{35} HH/C_{34} HH (0.59–0.72) and small homohopane indices (C_{35}HH/C_{31}HH-C_{35}HH), ranging between 0.06 and 0.07.

In sector 3, the analyzed samples (OS9, OS10) have a higher abundance of pentacyclic terpanes than tricyclic terpanes (Fig. 10), with ratios of tricyclic (tr) to pentacyclic terpanes (H) materialized by low C_{23}tr/C_{30}H ratios ranging from 0.11 to 0.66 (Table 5). In almost the analyzed samples, the dominant peak of tricyclic terpanes is C_{23}tr, showing an ascending trend of $C_{19}tr < C_{20}tr < C_{21}tr < C_{23}tr$. The C_{19}tr/C_{23}tr, and C_{24}Tet/C_{26}tr ratios are low ranging from 0.10 to 0.17 and from 0.53 to 0.57. C_{26}tr/C_{25}tr ratios are relatively high in the range of 0.88–1.02 (Table 5).

The conventional hopane with a carbon number of 30αβH (C_{30}-17α, 21β hopane) is the dominant peak in the analyzed oil seep samples. There are few rearranged hopanes, only a small amount of C_{29}Ts (C_{29}-18α-neohopanes) and an extremely small amount of 30 Diah (C_{30}-17α-diahopanes) that were detected (Fig. 10). The content of gammacerane is low (GI = 0.02–0.13). The hopane distribution patterns of samples are characterized by a regular stair-step progression of C_{31} to C_{35} homohopanes (C_{31}HH-C_{35}HH) with the predominance of 22S over 22R epimers. These samples display low to fair C_{35} HH/C_{34} HH (0.68–1.00) and small homohopane indices (C_{35}HH/C_{31}HH-C_{35}HH), ranging between 0.07 and 0.09.

In sector 1, the OS3 sample shows C_{29} regular steranes which are dominant over C_{27} and C_{28} steranes (C_{29}ααR/C_{27}ααR ratios in the order of 1.33). The rest of the oil seep samples (OS1 and OS2) have no C_{27} or C_{29} predominance (C_{29}ααR/C_{27}ααR: 0.96–1.03). The C_{27}, C_{28}, and C_{29} regular steranes contents are in the range of 34–43%, 24–31%, and 26–39%, respectively (Fig. 11; Table 5). The C_{27}diasterane/C_{27} regular sterane (C_{27}βα (R + S)/C_{27} αα (R + S)) ratios of the analyzed samples fluctuate between 0.58 and 1.39. Among these samples, OS1 displays the lowest C_{27}βα (R + S)/C_{27} αα (R + S) value in the order of 0.58 indicating relatively low diasterane contents.

In sector 2, the relative abundance of regular steranes (C_{27}, C_{28}, and C_{29}) differs greatly among oil seep samples. For OS4 and OS5 samples, there is no C_{27} or C_{29} predominance (C_{29}ααR/C_{27}ααR: 0.99–1.22).

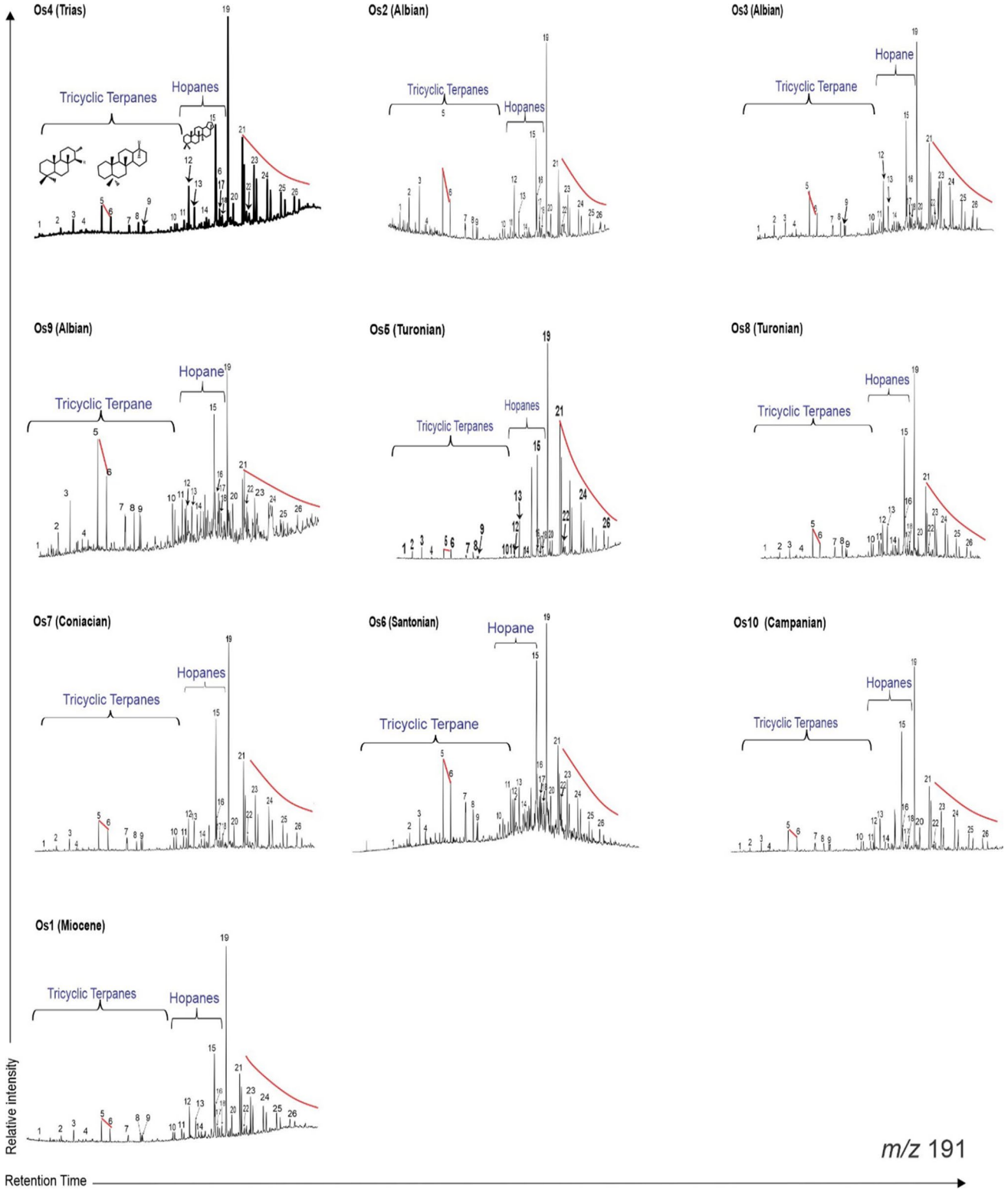

Fig. 10 Mass chromatograms showing the distribution of terpanes (*m/z* 191) of selected oil seep samples (for key, see Table 3)

For the OS6, OS7, and OS8 oil seep samples, the C_{29} regular steranes are dominant over C_{27} and C_{28} steranes ($C_{29}\alpha\alpha R/C_{27}\alpha\alpha R$ ratios range from 1.10 to 1.86). The C_{27}, C_{28}, and C_{29} regular steranes contents are in the range of 29–35%, 26–34%, and 32–47%, respectively (Fig. 11; Table 5). In sector 3, for the OS9 sample, the C_{27} regular steranes predominate over C_{28} and C_{29} steranes ($C_{29}\alpha\alpha R/C_{27}\alpha\alpha R = 0.88$). The OS10 sample has no C_{27} or C_{29} predominance ($C_{29}\alpha\alpha R/C_{27}\alpha\alpha R$: 0.91). The C_{27}, C_{28}, and C_{29} regular steranes contents are in the range of 37–44%, 21–23%, and 36–40%, respectively (Fig. 11; Table 5).

The sterane distribution (*m/z* 217) indicates the lowest value of C_{27}diasterane content, with high values of $C_{29}\alpha\alpha\alpha 20S/(20S + 20R)$ (0.36) and $C_{29}\alpha\beta\beta/(\alpha\beta\beta + \alpha\alpha\alpha)$ (0.50) in OS1 sample (Table 5) while, OS2 and OS3 samples display the highest C_{27}diasterane content and $C_{29}\alpha\alpha\alpha 20S/(20S + 20R)$ and $C_{29}\alpha\beta\beta/(\alpha\beta\beta + \alpha\alpha\alpha)$ in the range of 0.52–0.57 and 0.49–0.54, respectively (Table 5).

The aromatic biomarkers (Table 5) show a low value of TAS (between 0.15 and 0.37) in OS1, OS2, and OS3 samples.

The C_{27}diasterane/C_{27} regular sterane ($C_{27}\beta\alpha$ (R + S)/C_{27} $\alpha\alpha$ (R + S)) ratios of the OS4, OS5, OS6, OS7, and OS8 samples fluctuate between 0.17 and 1.80. The OS5 and OS7 samples display the lowest $C_{27}\beta\alpha$ (R + S)/C_{27} $\alpha\alpha$ (R + S) values ranging from 0.17 to 0.81 and indicating relatively low diasterane contents with C_{29} $\alpha\alpha\alpha 20S/(20S + 20R)$ (0.46–0.69) and $C_{29}\alpha\beta\beta/(\alpha\beta\beta + \alpha\alpha\alpha)$ (0.57–0.57), respectively (Table 5). However, OS4, OS6, and OS8 samples display the highest C_{27}diasterane content, C_{29} $\alpha\alpha\alpha 20S/(20S + 20R)$ in the order of 0.43–0.58, and $C_{29}\alpha\beta\beta/(\alpha\beta\beta + \alpha\alpha\alpha)$ in the range of 0.46–0.53, respectively (Table 5). Additionally, the aromatic biomarkers (Table 5) show a low value of TAS (0.07) in the OS5 sample from the borehole mine in sector 2 whilst the TAS values of samples collected from the surface range between 0.16 and 0.32.

The OS9 sample displays the highest C_{27}diasterane content with high $C_{27}\beta\alpha$ (R + S)/C_{27} $\alpha\alpha$ (R + S) value (in the order of 1.9), C_{29} $\alpha\alpha\alpha 20S/(20S + 20R)$, and $C_{29}\alpha\beta\beta/(\alpha\beta\beta + \alpha\alpha\alpha)$ ratios in the order of 0.42–0.46, respectively (Fig. 11; Table 5), while the OS10 one shows the lowest C_{27}diasterane content with the lowest $C_{27}\beta\alpha$ (R + S)/C_{27} $\alpha\alpha$ (R + S) values (0.75) and C_{29} $\alpha\alpha\alpha 20S/(20S + 20R)$, and $C_{29}\alpha\beta\beta/(\alpha\beta\beta + \alpha\alpha\alpha)$ ratios (in the order of 0.41), respectively (Table 5).

The aromatic biomarkers (Table 5) for OS9 and OS10 samples of the borehole mine in sector 3 show TAS values varying between 0.01 and 0.03.

On the other hand, the oil-oil correlation using the $C27\beta\alpha S/C27\alpha\alpha S$ versus $C_{29}H/C_{30}H$ (Fig. 14a) and $C_{27}\beta\alpha S/C_{27}\alpha\alpha S$ versus $C_{24}Tet/(C_{24}Tet + C_{23})$ diagrams (Fig. 14b) shows the existence of three oil families marked by the difference of depositional environment and lithology.

Discussion

Richness, hydrocarbon generation potential, and typing of OM

In the studied sectors (1 and 2), the upper Albian lower Fahdene and the Cenomanian–Turonian Bahloul Fms are marked by moderate to good and moderate to excellent OM richness up to 4.78 wt.% and 8.10 wt.% TOC with a mean of 0.90 wt.% and 3.5 wt.% indicating fair to good and good to the excellent quality of the OM preserved in these Fms, respectively.

The TOC contents vary widely between samples and localities (Table 4): the highest TOC contents occurred in the middle and the upper parts of the Fahdene Fm, while the highest TOC contents characterize the lower (U1) and upper (U3) units of the Bahloul Fm.

The lateral variations suggest differences in palaeodepositional settings between the localities, resulting in the decreasing TOC trend from NW to SE in sector 1 and the increasing TOC from NE to SW in sector 2 for the Fahdene Fm, while TOC variations show a slightly increasing from NE to SW in sector 1 and from South to North in sector 2 for the Bahloul Fm (Table 4).

According to the fact that TOC concentrations on the seafloor may record variations in surface bioproductivity and/or OM preservation during sedimentation and early diagenesis, the Fahdene and Bahloul Fms are considered to be deposited in a marine basin which was controlled by the interplay of subsidence and synsedimentary faults in tilted blocks associated with Triassic salt tectonics (Morgan et al. 1998; Grasso et al. 1999; Patriat et al. 2003; Soua et al. 2009; Hallek et al. 2019; Talbi et al. 2021; Ben Ammar et al. 2021). Thus, the highest average TOC contents in the studied sites (Table 4) coincide with subsiding zones (grabens and half-grabens) located around Triassic salt diapirs.

Additionally, in sector 1, the PP values registered in the Fahdene Fm of Jebel Rihane (JR-LF) are widely variable throughout the lithological column ranging from 0.11 to 2.40 mg HC/g rock, 1.96 to 3.36 mg HC/g rock, and 0.55 to 4.87 mg HC/g rock in the basal, middle, and upper units, respectively depending on their primary OM-richness and maturity level.

In the Oued Siliana section (OS-LF), located in the same sector 1, the PP ranges between 0.09 and 3.44 mg HC/g rock, with a mean of 1.03 mg HC/g rock indicating fair to good source rock, while in sector 2, the PP of the Fahdene Fm in Lakhaouat locality varies from 1.06 to 5.10 with a mean of 2.82 mg HC/g rock (Table 4). On the other hand, the S2 versus TOC plot (Fig. 12a) confirms that most samples display fair to good TOC contents and PP values indicating a fair to good source rock.

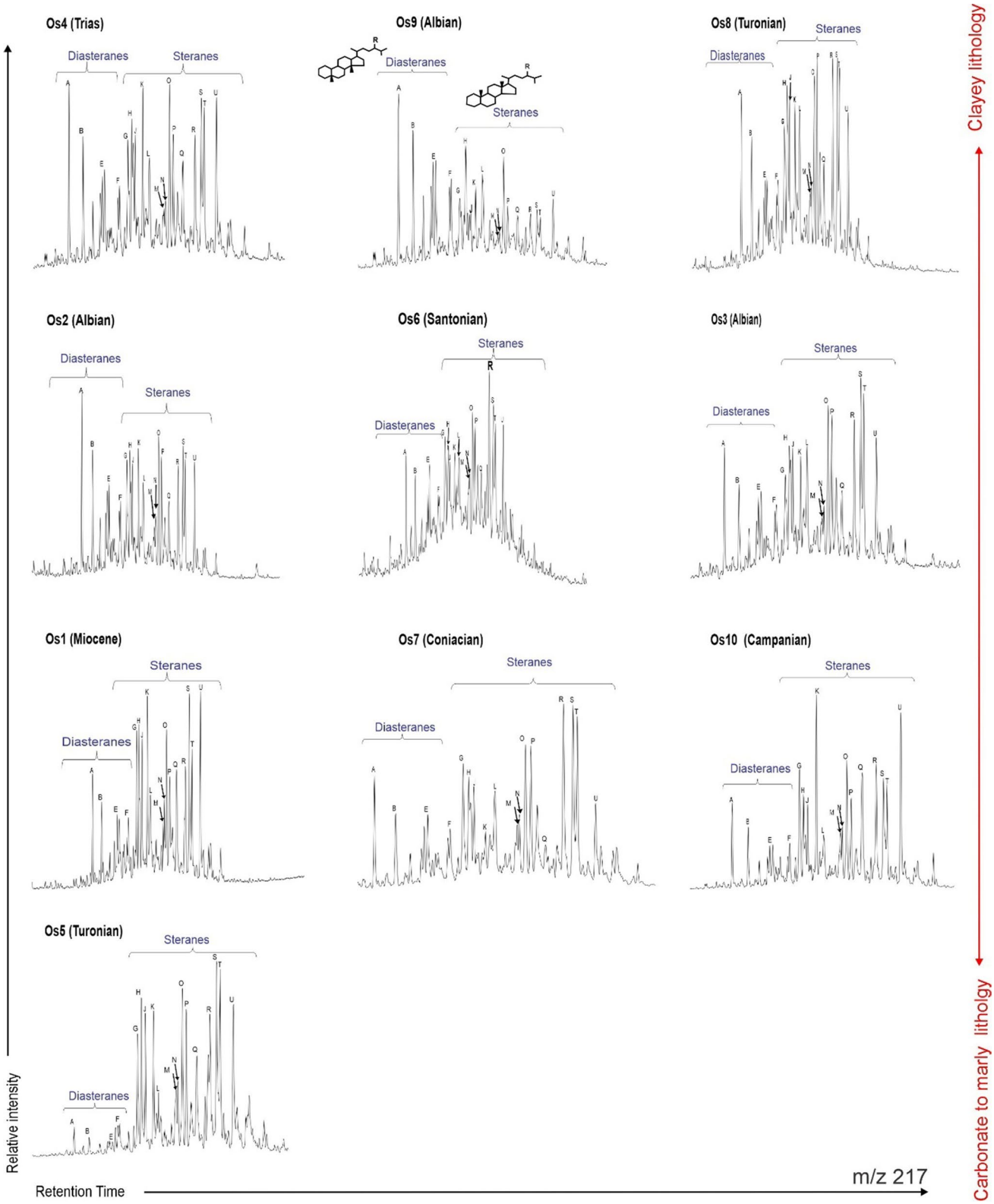

Fig. 11 Mass chromatograms showing the distribution of steranes (*m/z* 217) of selected oil seep samples (for key, see Table 3)

The PP values of the Bahloul Fm are also variable throughout the lithological column (Fig. 7). This can be clearly seen in the Oued Siliana section (OS-BH) in sector 1 where PP values range between 1.5 and 18.61 mg HC/g rock, 2.61 and 6.39 mg HC/g rock, and 0.45 and 9.12 mg HC/g rock in the lower (U1), middle (U2), and upper (U3) units, respectively, displaying a moderate to very good source rock.

In the Kenana section (KN-BH), the PP values range between 4.34 and 29.44 mg HC/g rock with a mean of 9.89 mg HC/g rock which indicates a good to very good source rock.

In sector 2, samples collected from Oued Merir (OMR-BH) show PP values ranging between 2.27 and 67.43 mg HC/g rock, while in the Lakhaouat section and Lakhaouat mine, they vary between 20.73 and 43.51 mg HC/g rock and 8.56 and 34.48 mg HC/g rock, respectively which is compatible with a good to the excellent source. The cross-plot S2 versus TOC (Fig. 12c) used for source quality and quantity assessments (Espitalie et al. 1985) shows fair to excellent TOC contents for the Bahloul Fm.

On the other hand, these mid-Cretaceous source rocks present variable HI and OI values (Table 4) depending on the quality and the preservation rate of OM. In this sense, the lower Fahdene Fm in the studied sections (sectors 1 and 2) shows relatively low HI (between 31 and 386, mean: 179 mg HC/g TOC) and low to high OI (6–220, mean: 64 mg CO_2/g TOC) values typical of mixed marine and terrestrial type II-III kerogen and an advanced maturity level with local alteration of OM, respectively (Peters 1986; Peters and Cassa 1994) (Fig. 12b).

Moreover, the extracted samples of Fahdene Fm (JR-LF9 and OS-LF4 from sector 1 and LK-LF5 from sector 2) exhibit the high Pr/Ph, Pr/n-C_{17}, and Ph/n-C_{18} ratios typical for a source rock with high contribution of terrestrial OM. Furthermore, the low GI and C_{35}/C_{34}-homohopanes ratios indicate a marine input of OM deposited under suboxic conditions with normal salinity water column (Peters and Moldowan 1993). The high abundance of C_{23}tr, C_{22}tr/C_{21}tr, and C_{26}tr/C_{25}tr and the lowest to medium ratios of C29H/C30H and regular diasteranes over steranes (Table 5) are consistent with a marine argillaceous carbonate depositional environment (Waples and Machihara 1991).

For the Bahloul samples, HI values are fair to high (HI: 230–703, mean: 458 mg HC/g TOC) and OI are low (mean OI: 31 mg CO_2/g TOC) which is compatible with a primarily marine type II OM (Fig. 12d).

Likewise, the extracted samples of Bahloul Fm (OS-BH33 from sector 1 and OMR-BH3 and LKM-BH2 from sector 2) show the low Pr/Ph, Pr/*n*-C_{17}, and Ph/*n*-C_{18} ratios typical of source rock with high contribution of marine algal-OM. Additionally, the low GI and C_{35}/C_{34}-homohopanes ratios suggest a marine input of OM deposited under suboxic conditions with normal salinity water column (Peters and Moldowan 1993).

On the other hand, the high abundance of the C_{23}tr and high $C_{29}H/C_{30}H$ ratio with the low C_{22}tr/C_{21}tr and C_{26}tr/C_{25}tr, and the regular steranes over diasteranes (Table 5) are indicative of OM deposited in a carbonate-marl marine environment (Waples and Machihara 1991).

Thermal maturity of source rocks

The thermal maturity of OM in the analyzed rock samples is evaluated based on T_{max} and production Index (PI) values (e.g. Tissot and Welte 1984; Waples 1985; Moldowan et al. 1986; Peters and Moldowan 1993) as well as on stereoisomerization ratios (Mackenzie et al. 1980; Peters et al. 2005).

The high T_{max} (441–459 °C) and PI (0.1–0.3) values of the lower Fahdene Fm outcropping in sector 1 reflect the OM in Jebel Rihane and Oued Siliana sections are mature (Oil window). However, in sector 2, the T_{max} values in the Lakhaouat section range between 428 and 439 °C with a mean of 432 °C and low PI (< 0.03) suggesting immature to marginally mature OM (Table 4; Fig. 12b).

The Bahloul source rock outcropping in sector 1 (Oued Siliana and Kenana localities) seems mature as indicated by the high T_{max} (435–446 °C; Table 4) and PI values (0.03–0.23; Table 4) whereas, toward sector 2 (Oued Merir and Lakhaouat localities), the Bahloul Fm, characterized by low T_{max} (< 435 °C) and PI (< 0.03) values, appears to be immature (Fig. 12d).

Regarding the biomarker maturity parameters, the high C_{29}20S/(20S + 20R) sterane and ββ/(ββ + αα) sterane ratios with a relatively high TAS registered in the lower Fahdene samples of Oued Siliana (OS-LF4) and Jebel Rihane (JR-LF9) in sector 1 (Table 5) indicate a mature source rock. Toward sector 2, the lower Fahdene of Lakhaouat section (LK-LF5) exhibits low 20S/(20S + 20R) sterane and ββ/(ββ + αα) C_{29} sterane ratios with low TAS values, confirming the low maturity level of OM (Table 5). Likewise, the extracted sample of the Bahloul Fm (OS-BH33) of Oued Siliana locality located in sector 1 exhibits the high 20S/(20S + 20R) sterane, ββ/(ββ + αα) C_{29} sterane, and TAS values attesting to the high maturity level of OM. However, toward sector 2, the extracted sample in the Oued Merir section (OMR-BH3) exhibits lower ratios of 20S/(20S + 20R) and ββ/(ββ + αα) C_{29} sterane, and low TAS values indicating a low maturity level of OM.

In sum, the OM preserved in Fahdene and Bahloul Fms is mature (late oil window) in sector 1 and immature in sector 2. This may be explained by the basin architecture which seems to be marked by the presence of subsiding zones in sector 1 and up-lifted ones near Triassic paleo-highs (i.e. Lakhaouat mine). Accordingly, a recent mineralogical investigation carried out by Jemmali et al. (2022) in the Lakhaouat Zn-Pb-(Ba-Sr) ore deposit, hosted mainly

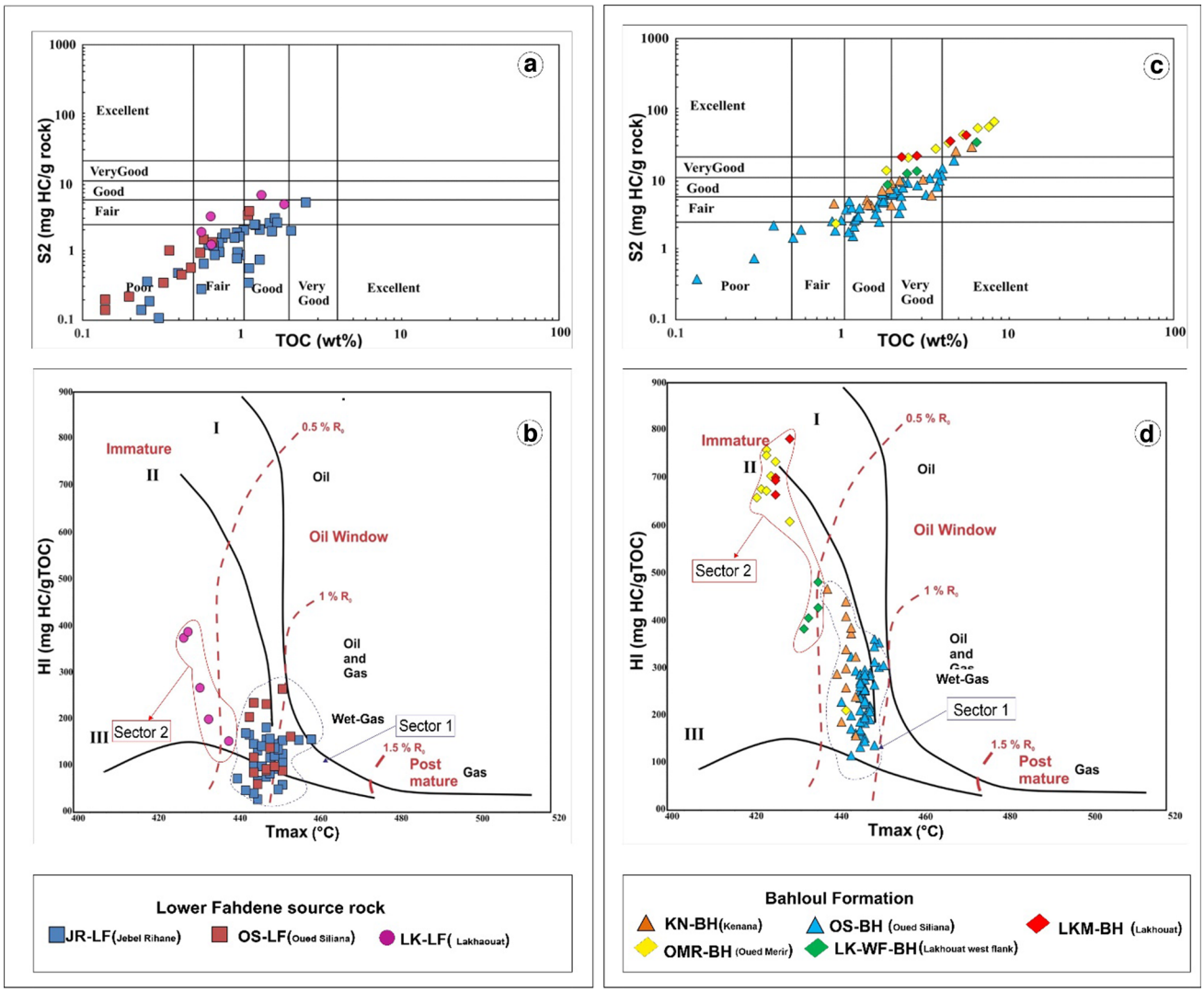

Fig. 12 S2 *vs.* TOC (**a**), HI *vs.* T_{max} (**b**) diagrams for the lower Fahdene Formation showing the richness and the maturity of organic matter. **c** S2 vs. TOC and **d** HI vs. T_{max} diagrams for the Bahloul Formation showing the richness and the maturity of organic matter

in the OM-rich Albian and Cenomanian–Turonian series, highlighted the presence of two types of fluid inclusions in calcite (Cal-2) corresponding to lower and higher maturities oils which were likely expelled at different stages of the Albian Fahdene and the Cenomanian–Turonian Bahloul source rocks.

Oil seeps and bitumen impregnations biomarkers signatures

Depositional environment

From n-alkanes and isoprenoids In the three studied sectors, most oil seeps samples (OS1, 2, 4, 5, 6, 8, 9, and 10) show a unimodal *n*-alkanes distribution ranging between *n*-C_{12} and *n*-$C_{34}+$ and maximizing at *n*-C_{16} to *n*-C_{18} with relatively high abundance of *n*-C_{15} to *n*-C_{20} alkanes (Fig. 9) and generally low degree of waxiness which indicate a marine origin of the primary OM (Moldowan et al. 1994), except the OS4 sample which is characterized by a high waxy compatible with a terrestrial OM contribution (Peters and Moldowan 1993; Moldowan et al. 1994).

Two samples only (OS3 from sector 1 and OS7 from sector 2) are characterized by a bimodal *n*-alkanes distribution that maximizes at *n*-C_{25} and *n*-C_{35}, respectively (Fig. 9) with relatively high and low degrees of waxiness which suggest a high waxy nature with a contribution of terrestrial OM for OS3 sample and a marine source for the second (OS7 sample) (Peters and Moldowan 1993). Additionally, variations of Pr/*n*-C_{17} and Ph/*n*-C_{18} ratios between 0.20 and 1.01

and between 0.28 and 1.57, respectively (Table 5) indicate a primarily marine origin of OM with a significant algal contribution (Peters and Moldowan 1993). Furthermore, the cross-plot of these values on a diagram Pr/n-C_{17} vs. Ph/n-C_{18} (Fig. 13a) attests the studied oil seeps were generated from type II and type II-III OM sources.

On the other hand, all studied samples have no clear odd/oven carbon number predominance but with low (Pr/Ph < 1 for OS4, 5, 9, and 10) and relatively fair to moderate (1 < Pr/Ph < 1.75 for OS1, 2, 3, 6, 7, and 8) Pr/Ph values (Table 5) attesting to deposition and preservation of their source rocks under reducing (anoxic) and suboxic factors, respectively (Peters and Moldowan 1993; Moldowan et al. 1994; Peters et al. 2005). The anoxic depositional environments coincide with the southern flanks of Lakhaouat (OS4 and 5), Boukhil (OS9), and Fej Lahdoum (OS10) diapirs which are recognized as significant Zn-Pb sulfide ore deposits. These diapirs correspond to paleohighs occupied by Triassic salt domes with southern subsiding zones developed in local faulted blocks thus creating favorable environments for the accumulation and preservation of high quantities of OM.

From terpanes and hopanes (m/z 191) The higher abundance of pentacyclic terpanes than tricyclic terpanes, the low C_{19}tr/C_{23}tr ratios, and concentrations of gammacerane of all studied samples (OS1, OS2, and OS3 from sector 1, OS4, OS5, OS6, OS7, and OS8 from sector 2, and OS9 and OS10 from sector 3) (Table 5) indicate a marine origin of their source rocks with a normal salinity water column. The low to fair C_{35}HH/C_{34}HH ratios and small homohopane indices (C_{35}HH/C_{31}HH-C_{35}HH) suggest oxic to suboxic depositional conditions (Peters and Moldowan 1993) (Table 5).

Additionally, the relatively high C_{29} H/C_{30}H and the medium to high C_{24}Trt/C_{26}Tr ratios of OS1 (from sector 1), OS5 and OS7 from sector 2, and OS 10 from sector 3) indicate that these oil seeps were sourced from marine marly carbonate source rocks. However, the low C_{29}H/C_{30}H and the low to medium C_{24}Trt/C_{26}tr ratios, registered in OS2 and OS3 from sector 1, OS4, OS6, and OS8 from sector 2, and OS9 from sector 3, suggest a marine argillaceous carbonate-rich source (Peters et al. 2005).

From diasteranes and steranes In sector 1, the OS3 sample is characterized by C_{29} regular steranes which are dominant over C_{27} and C_{28} ones (C_{29}ααR/C_{27}ααR ratios in the order of 1.33), indicating a contribution of terrestrial OM in its source rock. The rest of the oil seep samples (OS1 and OS2) have no C_{27} or C_{29} predominance (C_{29}ααR/C_{27}ααR). The C_{27}, C_{28}, and C_{29} regular steranes contents are indicative of marine planktonic-bacterial OM as can be shown by the regular steranes distribution in the ternary diagram (Fig. 13b; Huang and Meinschein 1979). Among these samples, OS1 displays the lowest C_{27}βα (R + S)/C_{27} αα (R + S) value (Table 5) and relatively low diasterane contents indicating a marl-carbonate lithology of its source rock. Conversely, the OS2 and OS3 samples show the highest C_{27}βα(R + S)/C_{27}αα (R + S) ratio values attesting to the argillaceous carbonate marine/lacustrine OM.

In sector 2, the OS4 and OS5 samples are marked by the absence of C_{27} or C_{29} predominance (C_{29}ααR/C_{27}ααR: 0.99–1.22) which indicates that these oil seeps were generated from a marine OM. For the OS6, OS7, and OS8 samples, the C_{29} regular steranes are dominant over C_{27} and C_{28} steranes (C_{29}ααR/C_{27}ααR ratios range from 1.10 to 1.86), while the OS4 and OS6 samples have a similar value of C_{27}diasterane/C_{27} regular sterane than the OS2 and OS3 samples which is consistent with an argillaceous carbonate lithology of their source rocks. Unlike, the low values of C_{27}βα (R + S)/C_{27} αα (R + S) in OS5 and OS7 samples have a similar marl-carbonate source rock lithology to the OS1 sample from sector 1 (Fig. 13b; Huang and Meinschein 1979).

In sector 3, for the OS9 sample, the predominance of C_{27} regular steranes and C_{29}ααR/C_{27}ααR, and the highest values of C_{27}diasterane/C_{27} regular sterane (> 1) indicate an argillaceous marine source. However, the OS10 sample has no C_{27} or C_{29} predominance (C_{29}ααR/C_{27}ααR: 0.91), and the lowest ratios of C_{27}diasterane/C_{27} regular sterane which is indicative of a marly-carbonate lithology of its source rock which contains a marine planktonic-bacterial OM supported also by the regular sterane distribution in the ternary diagram of Huang and Meinschein (1979) (Fig. 13b).

Oil maturity

In sector 1, the sterane distribution (*m/z* 217), characterized by the high C_{29}ααα20S/(20S + 20R) and C_{29}αββ/(αββ + ααα) values indicates that the three studied samples (OS1, OS2, and OS3) were generated from source rocks containing mature OM (Table 5; Fig. 13c). This is confirmed by the highest TAS values in aromatic biomarkers (Table 5).

In sector 2, the OS5 sample collected from the Lakhaouat mine displays relatively low C_{29} ααα20S/(20S + 20R) and C_{29}αββ/(αββ + ααα), as well as low TAS aromatic values (Table 5) indicating an early mature stage of its source rock OM (Fig. 13c). Conversely, the OS4 (Lakhaouat mine) as well as OS6 and OS8 (SE of J. Ech-Cheid) samples, marked by the high C_{29}ααα20S/(20S + 20R) and C_{29}αββ/(αββ + ααα) and TAS values (Table 5), are generated from mature source rocks similar to those of sector 1 (Fig. 13c). Hence, we state,

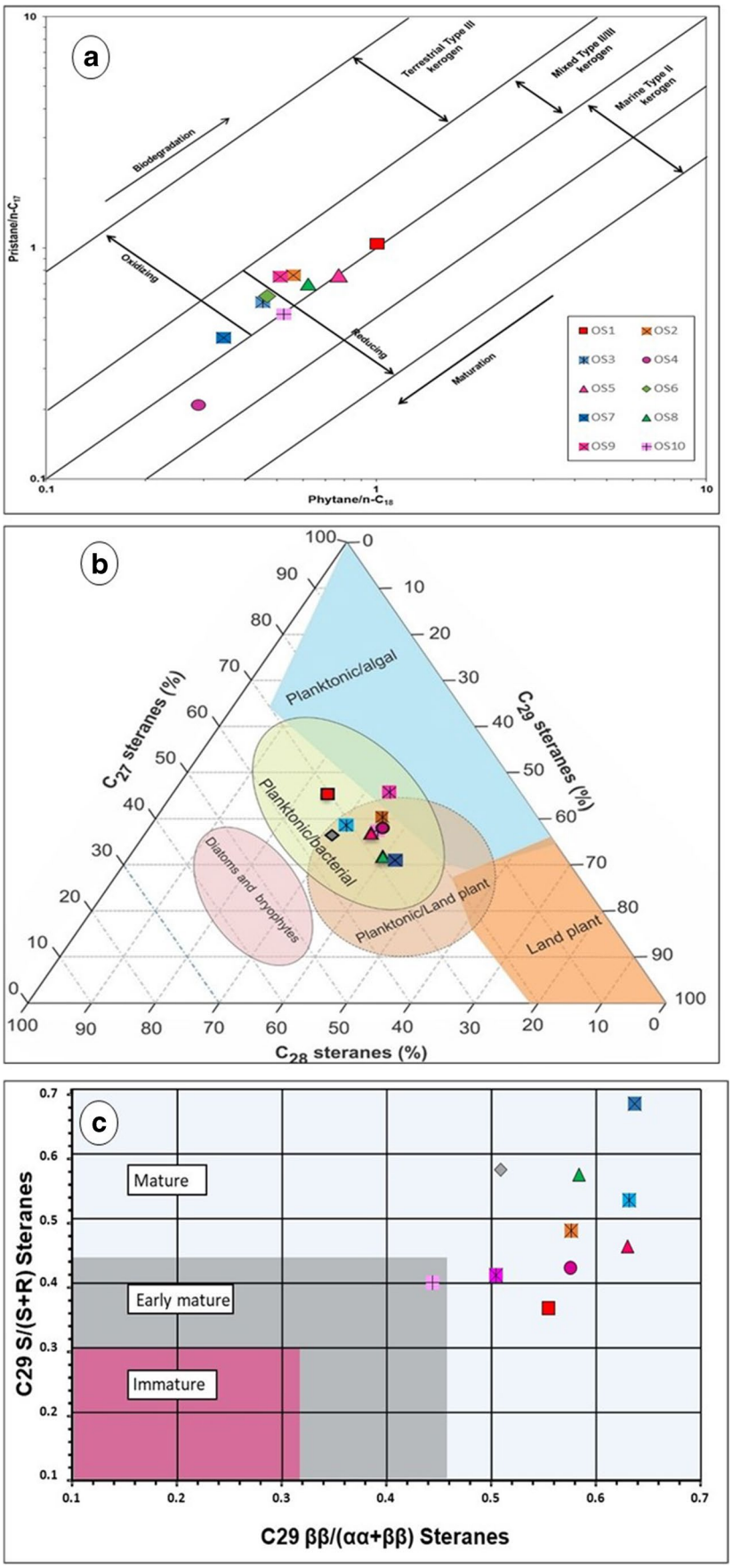

Fig. 13 **a** Cross-plot of Pr/*n*-C_{17} vs. Ph/*n*-C_{18} ratios of the studied oil seep samples (modified from Hunt 1995) showing the origin and the depositional environment of samples, **b** C_{27}: C_{28}: C_{29} regular steranes ternary diagram (modified after Huang and Meinschein 1979) showing the nature of the organic matter of the oil seep source rocks from Jebel Ech-Cheid and neighbouring structures. **c** Range of thermal maturity based on biomarker maturity ratios, i.e., $C_{29}S(S+R)$ steranes vs. $C_{29}\beta\beta(\alpha\alpha+\beta\beta)$ steranes showing the increasing thermal maturity of oil seep samples in the studied area

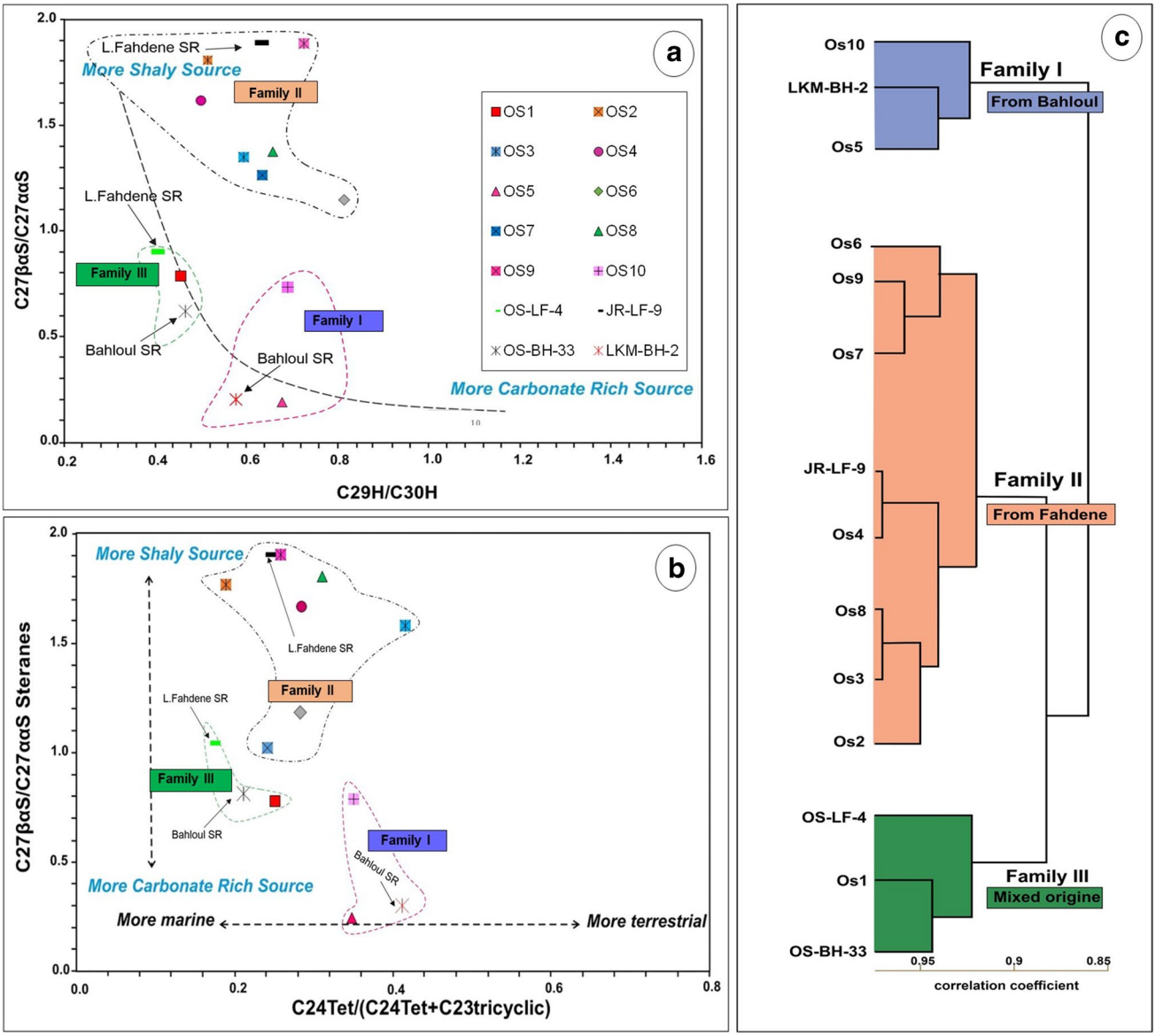

Fig. 14 **a** Cross-plot of $C_{27}\beta\alpha S/C_{27}\beta\beta S$ Hopanes vs. $C_{29}/C_{30}H$ Hopanes, **b** cross-plot of $C_{27}\beta\alpha S/C_{27}\beta\beta S$ Hopanes vs. C_{24}Tetracyclic/C_{24}Tetra + C_{23}tricyclic Terpanes Hopanes illustrating the oil family of the studied samples, and the hierarchical cluster analysis (HCA) dendrogram (**c**) showing the oil seep/source rock family

for a second time, the presence of low (OS5 sample) and high (OS4 sample) oil maturity stages in Lakhaouat mine, previously described by Jemmali et al. (2022) using a fluid inclusions investigation.

In sector 3, the OS9 sample (Fej Lahdoum mine) displays low $C_{29}\alpha\alpha\alpha 20S/(20S+20R)$, $C_{29}\alpha\beta\beta/(\alpha\beta\beta+\alpha\alpha\alpha)$, and TAS values (Table 5; Fig. 13c), attesting to early mature source rock, while the OS10 sample (Boukhil mine) exhibits the highest C_{29} $\alpha\alpha\alpha 20S/(20S+20R)$, $C_{29}\alpha\beta\beta/(\alpha\beta\beta+\alpha\alpha\alpha)$, and TAS values suggesting that this sample was sourced from a mature source rock (Table 5; Fig. 13c).

Oil-oil and oil-source rock correlation

Previous studies (e.g. Gurgey 2003; Peters 2005) showed that the alkanes, terpanes, and steranes biomarkers may be used for correlation purposes (Table 5) since these compounds are resistant to different transformation phenomena. Four mature source rock samples have been selected according to their high values of T_{max}, 20S/(20S + 20R) sterane, and $\beta\beta/(\beta\beta+\alpha\alpha)$ C_{29} sterane ratios.

The hierarchical cluster analysis (HCA) (Peters and Fowler 2002) has been used to classify oils with different

sources using the combination of different biomarker parameters (Fig. 14).

The obtained results show:

– The OS5 and OS10 samples from sectors 2 and 3, respectively, belong to the family I.

These oils are characterized respectively by (1) low values of $C_{27}\beta\alpha(R+S)/C_{27}\alpha\alpha(R+S)$ and C_{19}/C_{23} and moderate values of the gammacerane index, and (2) high values of Ts/Tm and $C_{29}\alpha\alpha\alpha20S/(20S+20R)$, which indicate that these oils are mature and appear to have been generated from a carbonate source rock deposited under anoxic conditions. Hence, they could be derived from the late Cenomanian-early Turonian Bahloul source rock;

– The OS2 and OS3 samples from sector 1 and OS4, OS6, OS7, and OS8 samples from sector 2, and OS9 sample from sector 3 belong to the second family (Family II). These are characterized by (1) low values of C_{19}/C_{23} (0.15–0.27) and gammacerane index (0.05–0.07), and (2) high ratio values of $C_{27}\beta\alpha(R+S)/C_{27}\alpha\alpha(R+S)$ (0.81–1.80), Ts/Tm (1.10–2.10), 20S/20S + 20R) (0.43–0.69), and C_{29} steranes $\beta\beta/(\beta\beta+\alpha\alpha)$ (0.52–1.80). The aforementioned results, suggesting a mature source rock derived probably from a clayey predominantly facies deposited in a dysoxic environment, could be correlated with the lower Fahdene source rock;
– The OS1 sample from sector 1 is classified in family III. It is characterized by the low gammacerane index, C_{19}/C_{23}, $C_{27}\beta\alpha(R+S)/C_{27}\alpha\alpha(R+S)$ values and the high Ts/Tm, 20S/20S + 20R), and C_{29} steranes $\beta\beta/(\beta\beta+\alpha\alpha)$ values. This attests to that this oil is mature and probably sourced from both the lower Fahdene and Bahloul Fms and or other source rock which can be the mid-upper Barremian M'Cherga Fm recently recognized northward as a good potential source rock (Talbi et al. 2021; Ben Ammar et al. 2021). However, the comparison of biomarkers from an upper Barremian source rock sample of Jebel Bazina (Ben Ammar et al. 2021) with those from the Rous-Essouani oil seep sample (OS 1) showed the absence of significant correlation, which could indicate either an over-mature stage (Gas window) of the OM fossilized in the Barremian facies or different migration pathways of the generated hydrocarbons from those of the upper Albian and the Cenomanian–Turonian facies.

Petroleum system assessment

In the studied area, the integration of our results on thermal maturity with the published data clearly indicates that the degree of thermal maturity of lower Fahdene and Bahloul Fms is quite low (immature) towards the SW part of Ech-Cheid (Lakhaouat mine) as indicated by the relatively low T_{max} values (in the range of 423 to 434 °C). Conversely, towards the northeast, the lower Fahdene (Upper Albian) and Bahloul (Cenomanian–Turonian) source rocks are mature to late mature as indicated by the relatively high T_{max} values ranging between 440 and 446 °C (Chaari 2002; Affouri et al. 2013; Layeb et al. 2013; Ben Fadhel et al. 2014; Talbi et al. 2021; present work), and oil maturity biomarker signatures (high $C_{29}\alpha\alpha\alpha20S/(20S+20R)$, $C_{29}\alpha\beta\beta/(\alpha\beta\beta+\alpha\alpha\alpha)$, and TAS values).

The increasing thermal maturity is attributed to the increased subsidence from the SW to the NE and the SE of the Ech-Cheid structure caused by regional tectonic movements along predominant NW–SE trending normal faults resulting from upper Cretaceous rifting. However, NE-SW inherited saliferous trends facilitated diapiric Atlassic structures. Minor N-S and E-W oriented faults are associated with the reactivation of deep faults inherited from Triassic-Jurassic Tethyan rifting. Such trends can be supported by oil seeps orientations along these directions (Chaari et al. 2003; Rddad et al 2019a, b). Hence, we consider that these directions may constitute the main pathways for oil migration from deeper to high domains. In fact, migration could occur along these faults and fractures in a convergent manner. For example, migration could be from NW to SE at the northern synform of the Ech-Cheid dome and from the SE to NW at the southern syncline, and the same for the other orientations. However, in the northern portion of sector 2, Cretaceous sediments, mainly of lower Fahdene and Bahloul Fms, were deposited near the paleohighs as a result of vertical movements of the Triassic salt dome in these locations since the lower Cretaceous (Layeb and Belayouni 1999; Jemmali et al. 2022). Hence, these potential source rocks were not buried enough to reach the maturity stage. The comparison of the geochemical results of the Cenomanian–Turonian and Albian facies according to a NE-SW transect extending from Oued Siliana shows that the thermal maturity decreases near the Triassic salt structure, whereas in the inter-diapiric zones, we notice an increase in the maturity level. In this context, as aforementioned above in the results section, the high maturity levels are registered in Jebel Rihane and Oued Siliana for the lower Fahdene Fm and in Oued Siliana, Kenana sites for the Bahloul Fm. These are considered to be the consequence of the interplay of subsidence and syn-sedimentary faults in tilted blocks associated with Triassic salt movements.

In summary, we state that the maturity level of mid-Cretaceous oil/gas source rocks is, here, mainly controlled by subsidence degrees in tilted blocks. For these reasons, Cretaceous sources could generate an amount/volume of HC that contributes to the charge of existent potential reservoir rocks around the area; this later could be middle-Turonian

Bireno, Coniacian Douleb, the Campanian–Maastrichtian Abiod carbonate, and Oum Dhouil Miocene reservoirs. Cretaceous, Paleocene, and Miocene argillaceous Fms form the main seals for the above-described reservoirs. These results encourage exploration of (1) buried structures (anticlines, uplifted zones) surrounding the Ech-Cheid area on one hand and (2) buried salt anomalies analogous in the Sahel domain and north-western Tunisia, on the other hand.

Conclusion

The geochemical investigation carried out on the upper Albian lower Fahdene and late Cenomanian-early Turonian Bahloul potential source rocks and ten oil seeps and bitumen impregnations collected from faulted Mesozoic and Cenozoic outcrops and mine boreholes located around three extrusive salt structures of Ech-Cheid, Fej Lahdoum, and Boukhil belonging to the Triassic salt domes zone of northern Tunisia allowed us to draw the following main remarks:

Rock–Eval pyrolysis highlighted fair to good quality of the Albian lower Fahdene (means TOC: 0.90 wt.%, HI: 180 mg HC/g TOC, and PP: 2.00 mg HC/g rock), and good to excellent quality of the Cenomanian–Turonian Bahloul Fms (TOC up to 8.1 wt.% with means TOC: 3.5 wt%, HI: 458 mg HC/g TOC, and PP: 20 mg HC/g rock reaching up to 67.43 mg HC/g rock). These source rocks were deposited in a deep marine basin marked by the presence of subsiding zones and paleohighs where OM accumulation and preservation were controlled by the interplay of global (eustatism, bioproductivity) and local factors among them subsidence and synsedimentary faults in tilted blocks associated with Triassic salt tectonics. The highest OM contents coincide with subsiding zones (grabens and half-grabens) located in the southern flanks of Triassic salt diapirs.

The basin architecture and the variable degrees of subsidence controlled the different maturity levels of the Fahdene and the Bahloul Fms between late diagenesis and the late oil window.

GC and GC–MS analysis of oil seeps and bitumen impregnations showed that these have been generated from mature and early-mature marine argillaceous and marl-carbonate source rocks deposited in oxic to suboxic and suboxic to anoxic environments with a normal salinity water column.

Biomarkers comparison and the depositional environment identification deduced from both extracts and oil seeps allowed the recognition of three oil families (I, II, and III). Families I and II correlated with the Albian lower Fahdene and the Cenomanian–Turonian Bahloul source rocks respectively, while family III is considered a mixture of hydrocarbons generated from both sources.

The spatio-temporal oil seeps distribution and their associated tectonics suggest several faults of NW–SE, N-S, E-W, and NE-SW trendings which facilitated oil migration from these source rocks to favorable upper Cretaceous and Miocene reservoirs.

Regarding these results, we state that Cretaceous petroleum systems are active in the study area. The maturation, expulsion, and migration have been realized but the trapping and preservation are the most critical processes. Future petroleum exploration should focus on research of aborted diapiric and anticline structures which could be found in inter-diapiric zones of north-western Tunisia, the Sahel basin, and the Pelagian block in eastern Tunisia.

Acknowledgements We are thankful to the engineers and staff of the "Entreprise Tunisiennne d'Activités Pétrolières" (ETAP) for their help during field and Lab work. Special thanks are addressed to Professor Larbi Rddad from the City University of New York and two anonymous reviewers for their pertinent comments that improved the scientific quality of the manuscript.

Declarations

Conflict of interest The authors declare that they have no competing interests.

References

Adil S (1993) Dynamique du Trias dans le nord de la Tunisie: bassins en relais multiples de décrochement, magmatisme et implication minière, Thèse de 3ème cycle, Univ. Tunis el Manar, Fac Sci Tunis 249 pp

Affouri H, Montacer M, Disnar JR (2013) Organic geochemistry of the Cenomanian- Turonian Bahloul Formation petroleum source rock, Central and Northern Tunisia. Res, Geol 63(3):262–287. https://doi.org/10.1111/rge.12008

Amri Z, Naji C, Masrouhi A, Bellier O (2020) Interconnection salt diapir–allochthonous salt sheet in northern Tunisia: the Lansarine-Baouala case study. J Afr Earth Sc 170:103876. https://doi.org/10.1016/j.jafrearsci.2020.103876

Arenillas I, Arz JA, Molina E, Dupuis C (2000) The Cretaceous boundary at Ain Settara, Tunisia: sudden catastrophic mass-extinction in planktic Foraminifera. J Foramin Res 30:202–218

Arfaoui MS, Khoun R, Dridi S, Zargouni F (2018) Style and timing of tectonic deformation across the Bou Arada-El Fahs troughs system, Northeast Tunisia: integration in the structural evolution of Atlas fold and thrust belt. Arab J Geosci. https://doi.org/10.1007/s12517-018-3436-3

Arthur MA, Glenn CR, Froelich PN (1988) Total dissolved CO2, alkalinity and 613C in pore waters of organic carbon-rich muds of the Peru margin. Geochim. Cosmochim. Acta (in prep)

Arthur MA, Jenkyns HC, Brumsack HJ, Schlanger, SO (1990) Stratigraphy, geochemistry, and paleoceanography of organic carbon-rich cretaceous sequences. In book: Cretaceous Resources, Events and Rhythms .pp.75–119. https://doi.org/10.1007/978-94-015-6861-6_6.

Bachari M, Grosheny D, Ferry S, France-Lonard C, Negra MH (2019) The Cenomanian-Turonian Boundary Event (CTBE) in north-central Tunisia (Jebels Serj and Bargou) integrated into regional data (Algeria to Tunisia). Cretac Res 94:108–125

Barrett P (1998) A comparative organic geochemical and stable isotope study of the Cenomanian– Turonian organic-rich sediments

from Tunisia, Germany and the UK. PhD thesis, University of Newcastle. 250 pp
Barrier E, Vrielynck B (2008) Paleotectonic maps of the Middle East," Middle East basins evolution program, CGMW, Atlas, 2008, Maps, pp. 1–14
Baudin F (2005) A Late Hauterivian short-lived anoxic event in the Mediterranean Tethys: the Faraoni Event: the 'Faraoni Event.' CR Geosci 337(16):1532–1540. https://doi.org/10.1016/j.crte.2005.08.012
Bédir M, Boukadi N, Tlig S, Ben Timzal F (2001) Subsurface mesozoic basins in the Central Atlas of Tunisia : tectonics, sequence deposit distribution, and hydrocarbon potential. AAPG Bulletin 85(5). https://doi.org/10.1306/8626CA2D-173B-11D7
Bédir M, Soltani A, Belhaj Mohamed A, Aribi A (2020) Cretaceous petroleum system modeling of Kairouan Basin in eastern Tunisia. Arabian J Geosci 13(14). https://doi.org/10.1007/s12517-020-05550-0
Behar F, Beaumont V, De B, Penteado HL (2001) Rock-Eval 6 Technology: performances and developments. Oil Gas Sci Technol Rev IFP 56(2):111–134. https://doi.org/10.2516/ogst:2001013
Bejaoui B, Solidoro C, Harzallah A, Chevalier C, Chapelle A, Zaaboub N (2017) 3D modeling of phytoplankton seasonal variation and nutrient budget in a southern Mediterranean Lagoon. Mar Pollut Bull 114:962–976
Belayouni H, Chandoul H, Mrad R (1992) Oil seep and associated phenomena in northern Tunisia. Field Trip guidebook, May 8–9, III^{èmes} Journées de Géologie Tunisienne Appliquée à la Recherche des Hydrocarbures. ETAP, Tunis 18 pp
Belhaj Mohamed A, Saidi M, Ben Jrad M, Saadani B (2015) The organic geochemistry of source rocks, bitumen, asphalts and oil stains from Northern Tunisia. Conference paper, 77 ^{the} EAGE conference and exhibition. https://doi.org/10.3997/2214-4609.201413144.
Ben Ammar S, Riahi S, Belhaj Mohamed A, Layeb M (2021) Source rock characterization of the upper Barremian, Albian and Cenomanian- Turonian organic-rich strata outcropping in Oued Bazina area, NE of Thibar diapir: Northern Tunisia. Arab J Geosci 13(24):21. https://doi.org/10.1007/s12517-020-06315-5
Ben Ammar S, Layeb M (2021) Updated geochemical insights on the Weissert and Faraoni events in the southern Tethyan margin (northern Tunisia). Arab J Geosci 14:2379
Ben Ayed N (1993) Evolution tectonique de l'avant-pays de la chaîne alpine de Tunisie du début du Mésozoïque à l'Actuel. Annales Des Mines Et De La Géologie, Tunisie 32:1–286. https://doi.org/10.1007/s12517-021-08669-w
Ben Ayed N (1994) Les décrochements-chevauchements EW et NS convergents de la Tunisie septentrionale: Géométrie et essai de reconstitution des conditions de déformation. Proceedings of the 4th Tunisian Petro. Exp. Conf., Tunisia, Expanded Abstracts, 25–37
Ben Chaabane N, Khemiri F, Soussi M, Latil JL, Emmanuel R, Belhaj Taher I (2018) Aptian-Lower Albian Serdj carbonate platform of the Tunisian Atlas: development, demise and petroleum implication. Mar Pet Geol 101:566–591. https://doi.org/10.1016/j.marpetgeo.2018.10.036
Ben Chalbi M, Kamel S, Harab S, Rebai N, Melki F, Meghraoui, M, Zargouni F (2014) Tectonisedimentary evidence in the Tunisian Atlas, Bou Arada Trough: Insights for the geodynamic evolution and Africa-Eurasia plate convergence. J Geol Soc 435-449. https://doi.org/10.1144/jgs2012-095
Ben Fadhel M, Zouaghi T, Amri A, Ben Youssef M (2014) Radiolarian and Planktic Foraminifera biostratigraphy of the Early Albian organic rich beds of Fahdene Formation, Northern Tunisia. Journal of Earth Science 25(1):45–63
Ben Fadhel M, Layeb M, Hedfi A, Ben Youssef M (2011) Albian oceanic anoxic events in northern Tunisia: biostratigraphic and geochemical insights. Cretac Res 32:685–699. https://doi.org/10.1016/j.cretres.2011.04.004
Ben Slama MM (2011) Mécanismes de mise en place du matériel salifère en Tunisie septentrionale: exemples du Jebel Ech-Cheid et des structures voisines, Thèse de 3^{éme} cycle, Univ, Tunis el Manar, Fac. Sci. Tunis, 116 pp
Bodin S, Godet A, Follmi KB, Vermeulen J, Arnaud H, Strasser A, Fiet N, Adatte T (2006) The late Hauterivian Faraoni oceanic anoxic event in the western Tethys: evidence from phosphorus burial rates: Palaeogeography, Palaeoclimatology, Palaeoecology 235(1–3):245–264. https://doi.org/10.1016/j.palaeo.2005.09.030
Bouaziz S, Barrier E, Soussi M, Turki MM, Zouari H (2002) Tectonic evolution of the northern African margin in Tunisia from paleostress data and sedimentary record. Tectonophysics 357(1–4):227–253. https://doi.org/10.1016/s0040-1951(02)00370-0
Bréhèret JG (1985) Sédimentologie et diagenèse de la matière organique contenue dons le niveau Paquier, couche repère de l'Albien inférieur du bassin vocon-tien (SE France). CR Acad Sc Paris II 301(15):1151–1156. https://doi.org/10.1016/0016-7037(80)90222-7
Burnett JA (1996) Nannofossils and Upper Cretaceous (sub-) stage boundaries state of the art. J Nannoplankton Res 18:23–32
Burollet PF (1956) Contribution à l'étude stratigraphique de la Tunisie centrale. Ann Mines Et Géol, Tunisie 18:1–352
Cecca F, Marini A, Pallini G, Baudin F, Begouen V (1994) A guide level of the upper most Hauterivian (Lower Cretaceous) in the pelagic succession of Umbria-Marche Apennines (Central Italy): the Faraoni Level. Riv Ital Paleontol Stratigr 99:551–568
Chaari G (2002) Geochemical study of the Late Albian and Cenomanian-Turonian source rocks: a key to assess the geodynamic evolution and the petroleum system of the Jebel Goraa area (salt dome zone, Northern Tunisia). DEA, Univ. Tunis El Manar, pp 1–135
Chaari G, Belayouni H, Soussi M (2003) Late Albian and Cenomanian-Turonian Source Rocks- A key to assess the geodynamic and the petroleum system of Jebel Goraa area−Salt Dome-Zone Northern Tunisia: 1st North African/Mediterranean Petroleum and Geoscience Conference and Exhibition. Tunis, 6–9, October, P043, pp. 1–6
Chihaoui A (2008) La transgression albienne dans la région de Tajerouine en Tunisie Centrale: Stratigraphie, sédimentologie et tectonique synsédimentaire [Doctoral dissertation]: Université Joseph-Fourier-Grenoble I
Dali (1994) Carte géologique 1/50 000 de Gaafour
Dercourt (2005) De l'Océan Téthysien à la Méditerranée : les phénomènes cataclysmiques, Académie des Inscriptions et Belles-Lettres, pp. 1–17
Durand-Delga M (1980) La Méditerranée occidentale, étapes de sa genèse et problèmes structuraux liés à celle-ci. Géol Soc Bull 10:203–224
El Euchi H, Saidi M, Fourati L, El Marhessi C (2004) Northern Tunisia thrust belt: deformation models and hydrocarbon systems, in: R. Swennen, F. Roure, J.W. Granath (Eds.), Deformation, fluidflow and reservoir appraisal in foreland fold-and-thrust belts, AAPG Hedberg 1: 371–380
Elkhazri A, Abdallah H, Razgallah S, Moullade M, Kuhnt W (2013) Carbon-isotope and microfaunal stratigraphy bounding the Lower Aptian Oceanic Anoxic Event 1a in northeastern Tunisia. Cretac Res 39:133–148. https://doi.org/10.1016/j.cretres.2012.05.011
Espitalie J, Deroo G, Marquis F (1985) La pyrolyse Rock-Eval et ses applications. Deuxieme Partie Rev Inst Franc Petrole 40(6):755–784
ETAP (2010) Tunisian stratigraphic chart
de Frizon Lamotte D, Mouchard A (2009) Mesozoic and Cenozoic vertical movements in the Atlas system (Algeria, Morocco, Tunisia): *An overview*. Tectonophysics 475:9–28. https://doi.org/10.1016/j.tecto.2008.10.024

Godet A, Hfaiedh R, Arnaud-Vanneau A, Zghal I, Arnaud H, Ouali J (2014) Aptian palaeoclimates and identification of an OAE1a equivalent in shallow marine environments of the southern Tethyan margin: evidence from Southern Tunisia (Bir Oum Ali section, Northern Chott Chain). Cretac Res 48:110–129. https://doi.org/10.1016/j.cretres.2013.12.006

Golonka J, Ford D (2000) Pangean (Late Carboniferous-Middle Jurassic) paleoenvironment and lithofacies. Palaeogeography, Palaeoclimatology, Palaeoecology 161:1–34. https://doi.org/10.1016/s0031-0182(00)00115-2

Golonka J, Kiessling W, Flugel E (2002) Plate-tectonic maps of the Phanerozoic SEPM (society for sedimentary geology) 72:21-75

Grasso M, Torelli L, Mazzoldi G (1999) Cretaceous-Palaeogene sedimentation patterns and structural evolution of the Tunisian shelf, offshore the Pelagian islands (central Mediterranean). Tectonophysics 315:235–250

Gurgey K (2003) Correlation, alteration, and origin of hydrocarbons in the GCA, Bahar, and Gum Adasi fields, western South Caspian Basin: geochemical and multivariate statistical assessments. Mar Pet Geol 20:1119–1139

Hadded A, Layeb M, Mennai-Tayech B, Benmadi M, Saidi M, Soussi M (2021) Subsurface geochemical and mineralogical evaluation for unconventional "shale" oil play of the Bahloul Formation (Cenomanian-Turonian) in the Sahel Basin Eastern Tunisia. Arab J Geosci 1701(14):1–30

Hallek T, Akrout D, Ahmadi R, Montacer M (2019) Assessment of sedimentary environment from PAHs and aliphatic biomarkers: the case study of Fahdene black shales in northern Tunisia. J Afr Earth Sci 161(4):103676. https://doi.org/10.1016/j.afrearsci.2019.103676

Hallek T, Montacer M (2021) Occurrences and origin of oil seeps and new marks of petroleum impregnations in Northwestern Tunisia: implications from aliphatic biomarkers and statistical modelling. J Afr Earth Sc 182(3):104278. https://doi.org/10.1016/j.jafreasci.2021.104278

Hamdi Naser I, Inoubli MH, Salem A, Tlig S (2009) Gravity contributions to the understanding of salt tectonics from the Jebel Cheid area (dome zone, Northern Tunisia). Geophys Prospect 57(4):719–728. https://doi.org/10.1111/j.1365-2478.2009.00788.x

Huang WY, Meinschein WG (1979) Sterols as ecological indicators. Geochimica and Cosmochimica Acta 43:739–745

Hunt JM (1995) Petroleum Geochemistry and Geology. Freeman, W.H., and Company, New York, USA, p 743

Jauzein A (1967) Contribution à l'étude géologique des confins de la dorsale tunisienne (Tunisie Septentrionale). Thèse ès Sciences-Annales des Mines et de Géologie, Tunis

Jemmali N, Rddad L, Sośnicka M, Rahali E, Souissi F, Carranza EJ (2022) Genesis of Zn-Pb-(Ba-Sr) mineralization in the Jebel El Akhouat deposit near the Ech Chehid salt diapir, Northern Tunisia. Petrol Mineral 116:71–91

Jenkyns HC (1988) The early Toarcian (Jurassic) anoxic event: stratigraphic, sedimentary, and geochemical evidence. Am J Sci 288(2):101–151. https://doi.org/10.2475/ajs.288.2.101

Jenkyns HC (2010) Geochemistry of oceanic anoxic events: Geochemistry, Geophysics, Geosystems 11(3):1–30. https://doi.org/10.1029/2009GC002788

Khalifa Z, Affouri H, Rigane A, Jérémy J (2018) The Albian oceanic anoxic events record in central and northern Tunisia: geochemical data and paleotectonic controls. Mar Pet Geol 93:145–166

Khomsi S, Bedir M, Soussi M, Ghazi Ben Jemia M, Ben Ismail-Lattrache K (2006) Mise en évidence en subsurface d'événements compressifs Eocène moyen-supérieur en Tunisie orientale (Sahel): généralité de la phase atlasique en Afrique du Nord. C R Geosci 338:41–49

Khomsi S, Soussi M, Mahersi C, Bedir M (2009) New insights on the structural style of the subsurface of the Tell units in north-western Tunisia issued from seismic imaging: geodynamic implications. Comptes Rendus Geosci 341(4):347–356. https://doi.org/10.1016/j.crte.2009.01.002

Klemme HD, Uimishek GF (1991) Effective petroleum source rocks of the world: stratigraphic distribution and controlling depositional factors. AAPG Bull 75(12):1809–1851. https://doi.org/10.1306/0C9B2A47-1710-11D7-8645000102C1865D

Klett TR (2022) Total petroleum systems of the Pelagian Province, Tunisia, Libya, Italy, and Malta; the Bou Dabbous. Tertiary Jurassic-Cretaceous Composite Bull 2202:149p. https://doi.org/10.3133/b2202D

Kuhnt W, Nederbragt A, Leine L (1997) Cyclicity of Cenomanian-Turonian organic-carbon-rich sediments in the Tarfaya Atlantic Coastal Basin (Morocco). Cretac Res 18:587–601. https://doi.org/10.1006/cres.1997.0076

Kuypers MM, Blokker P, Hopmans EC, Kinkel H, Pancost RD, Schouten S, Sinninghe Damste JS (2002) Archeaeal remains dominate marine organic matter from the early Albian oceanic anoxic event 1b. Palaeogeography, Palaeoclimatology, Palaeoecology 185–211

Layeb M, Belyouni H (1989) La formation Bahloul au Centre-Nord de la Tunisie: un bel exemple de roche mère de pétrole à fort intérêt pétrolier. Actes des deuxièmes journées de géologie appliquée à la recherche des hydrocarbures, mémoire n 3, Tunis, pp. 489–503

Layeb M (1990) Etude géologique, géochimique et minéralogique régionale, des faciès riches en matière organique de la formation Bahloul (passage Cénomano-Turonien) en Tunisie Nord-Centrale. PhD Thesis, Faculty of Sciences of Tunis p. 209

Layeb M, Belayouni H (1999) Paléogéographie de la Formation Bahloul (passage Cénomanien-Turonien). Ann Min Géol 40:21–44

Layeb M, Ben Fadhel M, Layeb-Tounsi Y, Ben Youssef M (2013) First microbialites associated to organic-rich facies of the oceanic anoxic event 2 (northern Tunisia, Cenomanian-Turonian transition). Arab J Geosci 7(8):3349–3363

Leckie M, Bralower T, Cashma R (2002) Oceanic anoxic events and plankton evolution: biotic response to tectonic forcing during the mid-Cretaceous. Paleoceanogra 17:1–29

Luning S, Kolonic S (2003) Uranium spectral gamma-ray response as a proxy for organic richness in black shales: applicability and limitations. J Pet Geol 26(2):153–174. https://doi.org/10.1111/j.1747-5457.2003.tb00023.x

Luning S, Kolonic S, Belhadj EM, Belhadj Z, Cota L, Baric G (2004) Integrated depositional model for the Cenomanian-Turonian organic-rich strata in North Africa. Earth-Sci Rev 64(1–2):51–117

Mackenzie AS, Patience RL, Maxwell JR, Vandenbroucke M, Durand B (1980) Molecular parameters of maturation in the Toarcian shales, Paris Basin, France—I. Changes in the configurations of acyclic isoprenoid alkanes, steranes and triterpanes. Geochimica et Cosmochimica Acta, 44(11):1709–1721. https://doi.org/10.1016/0016-7037(80)90222-7

Mahjoub K, Dali T (1998) Carte géologique de la Tunisie à 1/50 000, feuille n°34, Bou Arada. Edit. Serv. Géol, Tunisie, ONM

Martinez C, Truillet R (1987) Evolution structurale et paléogéographique de la Tunisie. Mem Soc Géol Ital, 38

Masrouhi A, Ghanmi M, Ben Slama MM, Ben Youssef M, Vila JM, Zargouni F (2008) New tectono-sedimentary evidence constraining the timing of the positive tectonic inversion and the Eocene Atlasic phase in northern Tunisia: implication for the North African paleo-margin evolution. C R Geosciences 340:771–778

Masrouhi A, Bellier O, Koyi H, Marie Vela J (2013) The evolution of the Lansarine-Baouala salt canopy in the North African

Cretaceous passive margin in Tunisia. Geol Mag 150(5):835–861. https://doi.org/10.1017/S0016756812000763
Masrouhi A, Gharbi M, Bellier O, Ben Youssef M (2019) The Southern Atlas Front in Tunisia and its foreland basin: Structural style and regional-scale deformation. Tectonophysics 764:1–24. https://doi.org/10.1016/j.tecto.2019.05.006
Mejri F, Burollet PF, Ben Ferjani A (2006) Petroleum geology of Tunisia. Renew Synthesis ETAP Memoir 22:233
Melki F, Zouaghi T, Ben Chalbi M, Bedir M, Zargouni F (2010) Tectono-sedimentary events and geodynamic evolution of the Mesozoic and Cenozoic basins of the Alpine Margin, Gulf of Tunis, Northeastern Tunisia offshore, C R Geosc 342:741-753. https://doi.org/10.1016/j.crte.2010.04.005
Melki F, Zouaghi T, Harrab S, Casas Sainz A, Bedir M, Zargouni F (2011) Structuring and evolution of Neogene transcurrent basins in the Tellian foreland domain, North-Eastern Tunisia. J Geodyn 52:57–69
Melki F, Zouaghi T, Ben Chalbi M, Bedir M, Zargouni F (2012) Role of the NE-SW Hercynian master fault systems and associated lineaments on the structuring and evolution of the Mesozoic and Cenozoic basins of the Alpine margin, northern Tunisia. https://doi.org/10.5772/50145
Moldowan JM, Sundararaman P, Schoell M (1986) Sensitivity of biomarker properties to depositional environment and/or source input in the Lower Toarcian of SWGermany. Org Geochem 10(4–6):915–926
Moldowan JM, Dahl J, Huizinga B, Fago F (1994) The molecular fossil record of oleanane and its relation to angiosperms. Science 265:768–771
Morgan M A, Grocott J, Moody RTJ (1998) The structural evolution of the Zaghouan-Ressas Structural Belt, northern Tunisia. In: Macgregor DS, Moody RTJ, Clark-Lowes, DD (ed.) Petroleum geology of North Africa. Geological Society, London, Special Publication, 132: 405–422
Patriat M, Ellouz N, Dey Z, Gaullier JM, Ben Kilani H (2003) The Hammamet, Gabes and Chotts basins (Tunisia): a review of the subsidence history. Sediment Geol 15:241–262
Perthuisot V (1974) Carte géologique de la Tunisie à 1/50 000, feuille n°33, Teboursouk. Edit Serv Géol, Tunisie, ONM
Perthuisot V (1978) Dynamique et pétrogenèse des extrusions triasiques en Tunisie septentrionale, Thèse d'État, École Normale Supérieure, ERA 604-CNRS, pp.321
Peters KE (1986) Guidelines for evaluating petroleum source rocks using programmed pyrolysis. AAPG Bull 70:318–329
Peters KE, Moldowan JM (1993) The Biomarker Guide. Interpreting Molecular Fossils in Petroleum and Ancient Sediments. New Jersey: Prentice Hall, 483–664
Peters KE and Cassa MR (1994) Applied source rock geochemistry, chapter 5, part II. Essential elements 93–120
Peters KE, Fowler MG (2002) Applications of petroleum geochemistry to exploration and reservoir management. Org Geochem 33:5–36
Peters KE, Walters CC, Moldowan JM (2005) The biomarkers Guide: Biomarkers and isotopes in Petroleum Exploration and Earth History. Second ed, vol 2, Cambridge University Press 499–502
Philp RP (1985) Fossil Fuel Biomarkers Application and Spectra. Elsevier Science and Publishing Company, New York, p 294
Rabhi M, Ben Ayed N (1990) Mise en évidence d'une tectonique compressive d'âge Aptien supérieur en Tunisie centrale. Notes Serv Géol De Tunisie 56:89–98
Rddad L, Jemmali N, Carranza EJ, Wälle M (2019a) Organic matter and metal contents within the Cretaceous rocks of the Slata-Guern Halfaya area, North-Central Tunisia: Implication for ore genesis. Ore Geology Review, v 113:103070
Rddad L, Jemmali N, Sośnicka M, Cousens BL (2019b) The Genesis of the Salt Diapir-Related Mississippi Valley-Type Ba-Pb-(±Zn) Ore of the Slata District, Tunisia: the role of Halokinesis, Hydrocarbon Migration, and Alpine Orogenesis. Econ Geol 114(8):1599–1620
Reichelt K (2005) Late Aptian-Albian of the Vocontian Basin (SE-France) and Albian of NE-Texas: Biostratigraphic and palaeoceanographic implications by planktic foraminifera faunas. dissertation
Riahi S, Soussi M, Stow D (2021) Sedimentologic and stratigraphic constraints on Oligo-Miocene deposition in the Mogod Mountains, northern Tunisia: new insights for paleogeographic evolution of North Africa passive margin. Int J Earth Sci 110(1):1–36. https://doi.org/10.1007/s00531-020-01980-z
Rouvier H (1977) Géologie de l'Extrême-Nord Tunisien : tectoniques et paléogéographies superposées à l'extrémité orientale de la chaine nord-maghrébine, Thèse d'Etat, université´ Pierre-et-Marie-Curie (Paris 6), pp.898
Sageman BB, Rich J, Arthur MA, Dean WE, Savrda CE, Bralower TJ (1998) Multiple Milankovitch cycles in the Bridge Creek Limestone (Cenomanian-Turonian), Western Interior Basin; in Dean WE, Arthur MA (eds.), Stratigraphy and Paleoenvironments of the Cretaceous Western Interior Seaway, U.S.A., Soc. Econ. Paleont. Mineral. Concepts in Sedimentology and Paleontology 6:153–171
Saidi M (1993) Etude géologique et géochimique des roches mères Albo-Vraconiennes dans le domaine de la Tunisie Centro-Septentrionale. Université Tunis El Manar, Thèse de doctorat, p 246
Saidi M, Inoubli H, Ghenima R, Ben Nasr D (1998) Geochemical characteristics of source rocks in Tunisia. ETAP internal report
Saidi M (2003) Tunisian source rocks and oils: geochemical characteristics and oil-source rock correlation. Internal report, ETAP, Tunisia
Schlanger SO, Jenkyns HC (1976) Cretaceous oceanic anoxic events, causes and consequences. Geology 55(3–4):179–184
Scotese CR (2007) Earth History: The Evolution of the Earth System.project. PALEOMAP Project 134 Dodge, IL 60202
Soltani A, Negra MH, Khemiri F, Bachari M (2022) Significance of instabilities, erosion and sea level changes during Upper Cretaceous sedimentation in central Tunisia. J Afr Earth Sc. https://doi.org/10.1016/j.jafrearsci.2022.104468
Soua M (2014a) A review of Jurassic Oceanic anoxic events as recorded in the Northern Margin of Africa Tunisia. J Geosci 2(3):94–106. https://doi.org/10.12691/jgg-2-3-4
Soua M (2014b) Early Carnian Anoxic Event as recorded in the southern Tethyan margin, Tunisia: an overview. Int Geol Rev 56(15):1884–1950. https://doi.org/10.1080/00206814.2014.967315
Soua M, Chihi H (2014c) Optimizing exploration procedure using Oceanic Anoxic Events as new tools for hydrocarbon strategy in Tunisia. In book: Advances in Data, Methods, Models and Their Applications in Oil/Gas Exploration. pp.25–89. Edition: Chapter 2, Science Publishing Group
Soua M (2015) Cretaceous oceanic anoxic events (OAEs) recorded in the northern margin of Africa as possible oil and gas shale potential in Tunisia: an overview. Int Geol Rev. https://doi.org/10.1080/00206814.2015.1065516
Soua M (2016) Cretaceous oceanic anoxic events (OAEs) recorded in thenorthern margin of Africa as possible oil and gas shale potential in Tunisia: an overview. Int Geol Rev 58(3):277–320
Soua M, Mabrouk El Asmi A, Zaghbib-Turki D (2022) The Cenomanian–Turonian Boundary Event (CTBE) as recorded in the northern margin of Africa: palaeoceanography of the Oceanic Anoxic Event (OAE-2), North-Central Tunisia. International geology review
Talbi R (1991) Etude géologique et géochimique des faciès riches en matière organique d'âge Albien du bassin de Bir M'Cherga (NE de Tunisie) : déterminisme de leur genèse et intérêt

pétrolier de la région [Ph.D. thesis] : University de Tunis, pp.223
Talbi R, Lakhdar R, Smati A, Spiller R, Levey R (2018) Aptian-Albian shale oil unconventional system as registration of Cretaceous oceanic anoxic sub-events in the southern Tethys (Bir M'Cherga basin, Tunisia). J Pet Explor Prod Technol 9:1007–1022. https://doi.org/10.1007/s13202-018-0596-3
Talbi R, Amri A, Boujemaa A, Gabteni H, Spiller R, Levy R (2021) First evidence of the early Cretaceous oceanic anoxic events (MBE and OAE1a) in the southern Tethyan margin (NE-Tunisia): biostratigraphy and shale resource system. J Petr Explor and Prod 11(4):1559–1575
Talbot (2005) "Evidence for Triassic salt domes in the Tunisian Atlas from gravity and geological data" by Jallouli C, et al. Tectonophysics 396 (2005) 209–225. Tectonophysics 406(3): 249-254. https://doi.org/10.1016/j.tecto.2005.05.020
Tissot BP, Welte DH (1984) Diagenesis, catagenesis and metagenesis of organic matter. Petroleum Formation and Occurrence. Springer, Berlin Heidelberg, pp 69–73
Touati Z, Haji T (2018) Redox, productivity and Paleotectonic studies in the southern Tethyan Margin of northern Tunisia. Mar Pet Geol 99:310–322. https://doi.org/10.1016/j.marpetgeo.2018.10.021
Tribovillard N, Algeo TJ, Baudin F, Riboulleau A (2012) Analysis of marine environmental conditions based on molybdenum–uranium covariation—applications to Mesozoic palaeoceanography: Chemical Geology 324–325:46–58. https://doi.org/10.1016/j.chemgeo.2011.09.009
Veevers JJ, Powell CM, Collinson JW, Lopez-Gamundi OR (1994) Memoir of the Geological Society of America 184(1):331-353
Veevers JJ (2004) Gondwanaland from 650–500 Ma assembly through 320 Ma merger in Pangea to 185–100 Ma breakup: supercontinental tectonics via stratigraphy and radiometric dating. Earth Sci Rev 68(1–2):1–132
Vila JM (1995) Première étude de surface d'un grand '"glacier de sel"' sous-marin: l'Est de la structure Ouenza-Ladjbel-Meridef (confins algéro-tunisiens). Proposition d'un scenario de mise en place et comparaisons. Bulletin De La Société Géologique De France 166:149–167
Waples DW (1985) Geochemistry in petroleum exploration: Boston, international human resources development corporation, p.232
Ward JH (1963) Hierarchical grouping to optimize an objective function. J Am Stat Assoc 58:236–244
Wignall PB, Myers KJ (1988) Interpreting benthic oxygen levels in mudrocks: a new approach. Geology 16(5):452–455
Wignall PB (1994) Black shales: Oxford, Oxford University Press, p.130
Wignall PB, Morante R, Newton R (1998) The Permo-Triassic transition in Spitsbergen: d13Corg. chemostratigraphy, Fe and S geochemistry, facies, fauna and trace fossils. Geol Mag 135:47–62
Withjack MO, Schlische RW, Olsen PE (1998) Diachronous rifting, drifting, and inversion on the passive margin of central eastern North America: an analog for other passive margins: AAPG Bull 82:817–835
Yukler MA, Moumen A, Daadouch I, Bouhlel H, Meskini, A, Saidi M, Jarraya H (1994) Quantitative evaluation of the geologic and hydrocarbon potential of the Gulf of Gabès. In: Entreprise Tunisienne d'Activités Pétrolières (ed), Proceedings of the 4th Tunisian Petroleum Exploration Conference, Tunis. Memoir, 8:69–7.
Zargouni F (1978) Analyse structurale de la chaîne de Lansarine (zone des diapirs, Atlas tunisien). Bulletin De La Société Des Sciences Naturelles, Tunisie 13:97–104
Zghal I, Arnaud-Vanneau A (2005) The Hameima Formation. Aptian-Turonian events in Central Tunisia. Field trip guidebook– Géologie Alpine. Sér Spéc 5:101–104
Ziegler PA (1988) Evolution of the Arctic-North Atlantic and the Western Tethys. Volume 43. American Association of Petroleum Geologists. https://doi.org/10.1306/M43478